ESTIMATION OF USLE's C-FACTOR USING VEGETATION INDICES (VIs) FOR SOIL EROSION MODELLING IN LAKE BOSUMTWI BASIN, GHANA.

By

Seyram Kofi Loh. BSc (Hons)

A Thesis submitted to the Department of Wildlife and Range Management, Kwame Nkrumah University of Science and Technology in partial fulfilment of the requirements for the degree of

MASTER OF SCIENCE

IN

GEO-INFORMATION SCIENCE

Faculty of Renewable Natural Resources

College of Agriculture and Natural Resources

JUNE, 2012

DECLARATION

I hereby declare that this thesis submission is my own work towards the MSc and to the best of my knowledge; it contains no material previously published by another person or material which has been submitted for any other degree of the university, except where due acknowledgement has been made in the text.

Seyram Kofi Loh	…….	…….
(Student)	Signature	Date

Certified by:

…….	…….	…….
(Supervisor)	Signature	Date
…….	…….	…….
(Supervisor)	Signature	Date
…….	…….	…….
(Head of Department)	Signature	Date

ABSTRACT

Water erosion is one of the most challenging environmental problems in Bosumtwi basin; this is due particularly to the rough terrain and human activities on the landscape. The Universal Soil Loss Equation (USLE) is a commonly used model in estimating soil loss by water. The USLE's cover and management factor (also known as *C* - factor) represents the combined effects of plant, soil cover and management on erosion. Therefore, this variable keeps changing as soil surface cover keeps changing. The use of remote sensing vegetation index to estimate *C* - factor proved to be reliable, consistent and useful when considering inaccessible and large regions. The normalized difference vegetation index *(*NDVI), is the most used algorithm in estimating the *C* - factor despite the availability of other indices believed to overcome some inherent problems associated with the use of NDVI. This study compares the NDVI to the EVI, in their capability to map land cover types, to be applied in *C*-factor estimation. Plots of the divergence statistics (derived from ISODATA clustering algorithm in ERDAS Imagine) against class numbers helped determine the optimal numbers the Hypertemporal vegetation index's (VI's) images can be classified into. The classification map outputs were reclassified based on the similarities of the profiles generated from the mean annual VI values. The resultant map of the supervised classification was compared to already classified map (produced from a single-date ASTER and data collected from the field) for legends assigning and validation. The overall accuracies of the two VI maps are both high (80 % or EVI and 70% for NDVI) and the kappa statistics of 0.7 and 0.5 for NDVI and EVI respectively. Forty-six (46) 2010 Hypertemporal MODIS EVI were applied in developing an annual *C*-factor model. In validating the model output; a *C*-map developed by

traditional method – based on EVI classified map and literature assigned *C* – values - was compared to the *C*-factor model developed using Exponential Function (E. F) approach. The *C*-factor model showed an overall accuracy of 76% and 0.6 kappa value.

Key words: Cover and management (*C*) factor, Erosion, Modeling, Vegetation Indices (*VIs*)

ACKNOWLEDGEMENT

First of all, I will like to thank the Almighty God for seeing me through this study. I will like to express my sincere gratitude to all my supervisors Dr. E. Westinga, Prof. W. Oduro and Mr. Ayer for their continuous supports and guidance throughout my research work. Dr. Westinga always supports my ideas regarding the study and offers the necessary guidelines. I am pleased about your patience in correcting my drafts. I appreciate Prof. Oduro for his insight remarks and the encouragements from the start of this work to the end. I also thank Mr. Ayer for his contribution especially with the technicalities of this work.

My sincere gratitude goes to Dr. M. Weir for his time and patience with me throughout every stage of this work; thus, development of proposal, field work, thesis writing and presentations. Similarly, I am grateful to Dr. L. van Leeuwen for her valuable suggestions during my research topic and study area searches and Dr. (Kees) de Bie for his contributions during my mid-term presentation. I thank also Mr L. Addae-Wereko and Mr. C. Kesse for being ever ready to help solve my challenges during the data analysis stage. Mr A. E. Gaizie, your support so immense, words cannot explain, God bless you all.

Last but not least, I am very grateful to all my family members for the encouragement and motivation during the difficult part of the study. My thanks go to Uncle Isaac, my mother, and siblings, God bless you all for the support.

TABLE OF CONTENTS

LIST OF TABLES

LIST OF FIGURES

LIST OF ACRONYMS

ASTER: Advanced Space-borne Thermal Emission & Radiation

AVHRR: Advanced Very High Resolution Radiometer

EVI: Enhanced Vegetation Index

GCP: Ground Control Points

GIS: Geo-Information Science

MODIS: Moderate Resolution Imaging Spectroradiometer NASA: National

Aeronautics & Space Administration NDVI: Normalized Difference Vegetation Index

NOAA: National Oceanic & Atmospheric Administration

TIR: Thermal Infrared Red

USGS: United States Geological Service UTM:

Universal Transverse Mercator

VI: Vegetation Index

ISODATA: Iterative Self-Organizing Data Analysis Technique

1.0 INTRODUCTION

1.1 Background

Soil erosion is a severe land degradation problem worldwide (Suriyaprasit & Shrestha, 2008). This sometimes occurs as a result of the removal of vegetation cover which influences erosion by reducing raindrop impacts on soil and the subsequent washing away. Soil erosion causes serious environmental degradation problems which hinder the development of agriculture and societies (Vaezi *et al.*, 2011). It also degrades soil quality, leading to siltation of reservoirs and flooding in low-lying zones in case of high rainfall events. In order to curtail these problems, sustainable conservation practices are adopted which entails in-depth understanding of the extent, risk and spatial distribution of soil erosion (Bewkert &Tefari, 2009; Wang *et al.*, 2009), and the most probable tools employed are predictive models (Suriyaprasit & Shrestha, 2008).

Erosion prediction models aid in long-range land management planning under natural and agricultural conditions (Vaezi *et al.*, 2011); and a frequently used one is the Universal Soil Loss Equation (USLE) (Wischmeier and Smith, 1978). The USLE model and its derivatives are commonly used to calculate average annual soil loss per unit land area resulting from rill and sheet (interrill) erosion. The USLE forms part of model category called empirical models and unlike the alternative group – physical models -; it is less data demanding, therefore, commonly used in data-scarce places (Bhattarai & Dutta, 2007). The USLE and its improved versions; the Modified Universal Soil Loss Equation (MUSLE) and the Revised Universal Soil Loss Equation (RUSLE) (Renard *et al.*, 1997), are also frequently used in predicting soil loss especially in watershed areas due to their ease of application (Lal 2001; Bhattarai & Dutta, 2007; Zhang *et al.*, 2009; Karaburun, 2010; Demirci & Karaburun, 2011).

Models and their factors affect very much the accuracy of the soil risk estimation (Karaburun, 2010). The USLE has six factors in its equation and estimates the average annual soil loss by a multiplicative relationship of these six (6) variables as depicted below:

$$A = R \ast K \ast S \ast L \ast C \ast P \cdots\cdots\cdots\cdots\cdots\cdots\cdots\cdots\cdots \ equation\ (1)$$

Equation 1: The USLE formula

where *A* is the estimated soil loss per year, R is the rainfall/runoff factor, *K* is the soil erodibility factor, LS is the slope length factor and steepness factor, *C* is the vegetation cover and management factor and the *P* represents the supporting conservation practice factor (Renard *et al.*, 1997). The *R* factor conveys the erosivity occurring from rainfall and runoff at a particular location. An increase in the intensity and amount of rainfall results in an increase in the value of *R*. The *K* factor expresses inherent erodibility of the soil and surface material. The *LS* factors express the effects of topography, specifically hillslope length and steepness factors, on soil erosion. An increased hillslope length and steepness factors result in increased *LS* factor, and correspondingly higher erosion. The *P* factor expresses the effects of supporting conservation practices, such as contouring, buffer strips of close growing vegetation, and terracing on soil loss at a particular site. These supporting conservation practices are measures taken to prevent erosion and they adjust the average annual soil loss accordingly. Lastly, the *C*-factor reflects the effects of cropping and management practices on soil erosion rates in agricultural lands, and also, the effects of vegetation canopy and ground covers on reducing forest soil erosion (Renard *et al.,* 1997).

The vegetation cover and management (*C*)-factor measures the combined effects of

interrelated cover and management variables; factors readily altered by human activities (Folly, *et al.*, 1996; Karaburun, 2010). Vegetation cover is the second most essential factor, after topography, in determining soil erosion vulnerability (van der Knijff, *et al.*, 1999). It acts as a buffer between the atmosphere and the soil (Erencin, 2000) and this effect is embedded in the *C* - factor of the (Revised) Universal Soil Loss Equation (USLE and RUSLE). The above-ground components of vegetation consisting of leaves and stems absorbs the impact of raindrops; while below-ground components involving root systems, add to the mechanical strength of soil against raindrop and surface flow influence. This significance of vegetation runs through other predictive models and is usually considered under the name of land cover/use and canopy cover information (Suriyaprasit & Shrestha, 2008). Human activities for instance agriculture extension and other land cover conversion activities that affect vegetation, invariably affects *C* - factor and soil erosion as well.

Traditionally, *C*-factor is determined from plot measurements and interpolation techniques, however, alternative approaches were established with the coming of remote sensing as a tool. The *C* - factor is empirically defined as the ratio of soil loss from land cropped under specific conditions to the corresponding loss from clean-tilled, continuous fallow (Wischmeier and Smith, 1978). The *C*-factor can be deduced through plot measurements on the field after which the non-sampled locations are estimated through spatial interpolation of the in situ measurements (Wischmeier and Smith, 1978). This approach is time-consuming, and computer intensive (Lu *et al.*, 2004), moreover, the interpolation outputs based on the sampled *C*-factor point values could be poor as a result of inadequate number of sample plots in complex environments (Wang *et al.*, 2002*b*).

The remote sensing satellite data as an important natural resource tool (Deng *et al.*, 2008) was therefore employed to prepare up to date information (Amiri and Tabatabaie, 2009). The *C*-factor specifically considers five sub-factors that explain the effects of prior land use, canopy cover, surface cover, surface roughness and soil moisture respectively as determined from the plot measurements (Renard *et al.*, 1997). However, remote sensing technologies cannot estimate all these parameters but they become useful when these data are not available due to inaccessibility problems in mountainous regions (Suriyaprasit & Shrestha, 2008); and also when continuous or large spatial data is required for a speedy jobs. Remote sensing land-cover classification was therefore adopted as an alternative option in deriving the *C*-factor (Millward and Mersey, 1999; Reusing *et al.*, 2000). This method is based on the assumption that same land covers have the same *C*-factor values.

The *C*-factor values are inferred from RUSLE guide tables or computed using field observation for each cover class and assigned to each pixel in the land cover class to form a *C*-factor map (Haan *et al.*, 1994). This classifications-based approach has some lapses as well, for instance, problems of classification inaccuracies, and land-cover classes details and also, appropriateness of the determined *C*-factor values for specific classes (Lu *et al.*, 2004). Furthermore, heterogeneous vegetation will likely have different *C*-factors even though it forms the same land-cover class with a common assigned *C*-factor value. These therefore led to the adoption of the vegetation indices-based approaches (Lu *et al.*, 2004). The spectral vegetation index (VI) method is a better method due to the representativeness of variation over the area under investigation (De Jong 1994; De Jong *et al.*, 1999; Wang *et al.*, 2002; Lin *et al.*, 2002).

1.1.1. Vegetation indices as an alternative to determine *C*-factor

There are two main approaches; the linear least square method (de Jong, 1994) and the exponential function method (Van der Kniff *et al.,* 1999). These are usually employed to convert indices into *C* -factor values; the latter was used in this study because of its superiority. Vegetation indices generally the normalized difference vegetation index (NDVI) is used to derive the cover (*C*) factor used in erosion modeling (Suriyapasit and Shrestha, 2008). There is a relationship between vegetation indices and *C*-factor. In 1994, de Jong explored the use of LANDSAT TM imagery for deducing vegetation properties like Leaf Area Index (LAI), percentage cover, and the USLE-*C* -factor. For this, as cited in (van der Knijff, *et al.*, 1999), areal estimations of percentage cover, LAI and *C* were determined from 33 plots in the Ardêche province in France. He compared the plot values with the corresponding NDVI-values on the TM-image (local average of a 150 by 150 m window around the plot location), giving regression equations that are able to estimate LAI, percentage cover and USLE-*C* from NDVI-values. De Jong (1994) deduced an equation for estimating USLE-*C* from NDVI (as cited in Van der Kniff *et al.*, 1999): A modest but significant correlation coefficient of -0.64 was realized. After several tests using NDVI profiles, *C*-values were found to be rather low; moreover, De Jong's model cannot predict *C*-values over 0.431. Additionally, the model was made for (semi-)natural vegetation types only, based on Landsat TM imagery consisting of varied spectral and geometric properties from MODIS images used here. Van der Knijff, *et al.*, (1999), investigated to find out if the NDVI-images could be "scaled" to approximate USLE-*C* values based on an alternative approach. Following several experimentations, equation (2) was arrived at:

$$C = \exp(-\alpha\left(\frac{NDVI}{\beta - NDVI}\right) \ldots\ldots\ldots\ldots\ldots\ldots\ldots\ldots\ldots\ldots \quad (2)$$

equation 2 is the Exponential function formula for calculating the *C*- factor

where: α, β are parameters that determine the shape of the NDVI-*C* curve. They suggested values of 2 and 1 for α and β respectively. Van der Knijff, *et al.*, (1999) also proven that the equation seems to produce more realistic *C* values than those estimated assuming a linear relationship. The value of *C* basically depends on the vegetation's cover percentage and growth stage (van der Knijff., *et al*, 1999). The *C*-factor of USLE ranges from 0 (meaning full very strong cover effect resulting in no erosion) to 1 (represents no vegetation cover effect) (Erencin, 2000), however the NDVI values range from 1 (full cover) to 0 (bare land), therefore, a relationship such as shown in figure (2) below is derived.

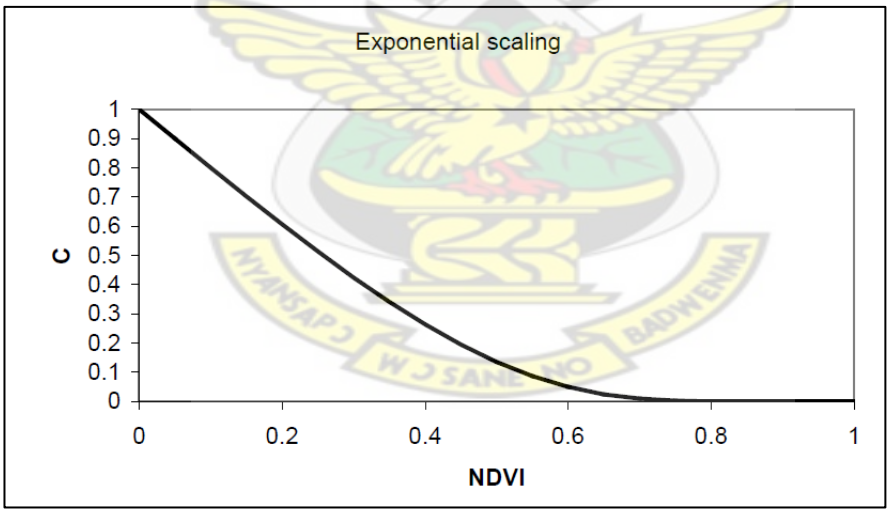

Figure 1: Showing the relationship between NDVI and USLE *C*-factor according to exponential scaling formula (Van der Knijff, *et al.*, 1999).

The exponential function as stated above was used by Gitas *et al.*, (2009) to convert multi-temporal *NDVI* layers from LANDSAT images into USLE *C*-factor for assessing erosion risk in N. Chalkidiki, Greece. Suriyaprasit and Shrestha, (2008), however stated

that *C*-factor values can be best assessed using field estimation and correlating them with NDVI *C*-factor values. They established this conclusion by plotting field measured 138 *C* - factor samples against NDVI *C*-factor values to transform NDVI into canopy cover values in Nam Chun watershed in Petchabun province of Thailand. An exponential relationship was established, afterwards, a regression function was applied to estimate a curve. Dependability of the *C* - factor map was assessed based on 125 independent validation data. The coefficient of efficiency of 0.77(where 1 is the best prediction) and a lower root mean square error (0.03) were calculated.

1.1.2. Vegetation indices background

This study makes use of two indices: the MODIS Normalized Difference Vegetation Index (NDVI), and the Enhanced Vegetation Index (EVI). The NDVI is one of the oldest, well known, and most frequently used VI. The combination of its normalized difference formulation and use of the highest absorption and reflectance regions of chlorophyll make it robust over a wide range of conditions. The NDVI can however saturate in dense vegetation conditions when LAI becomes high. The EVI is believed to improve greatly on this problem of the NDVI. These two indices are produced by the MODIS team to complement each other. A brief history of vegetation algorithms is found below.

Retrieving vegetation index's information from remotely sensed data

Vegetation index (VI) is mainly characteristic of electromagnetic radiations of (green) land cover types and is therefore useful in establishing the status of these ground covers. The VI is a value that is calculated from sets of remotely sensed data on the basis of spectral distinction between bands as observed from vegetation and other land covers. Vegetation is typically characterized by strong absorption in the red wavelengths and high reflectance in the near infra-red (NIR) wavelengths of the

electromagnetic spectrum. There are considerable absorption of sunlight in the red-light region of the electromagnetic spectrum by plant's chlorophyll cells and the reflectance of the near-infra (NIR) portion of the electromagnetic spectrum by the leaf's spongy mesophyll structures results in a distinctive contrast in spectral behavior; this forms the background of VIs in the history of terrestrial remote sensing (Gitelson, 2004). The reflectance properties of plants change as canopy changes seasonally. Profiles generated from multi-temporal VI images can characteristically give information about ground conditions. Studies therefore apply this to analyze health of vegetation in a place relative to the norm (*USGS website*). Vegetation indices can reveal fluctuations in vegetation cover due to human activities such as deforestation, natural disturbances such as wild fires, or changes in plants' phenological phase (*USGS website*). Tucker (1979) first discovered that the Simple Ratio (as it was later called), made of a ratio of Red and near Infrared (NIR) and the linear combinations of same reflectance's (e.g.. ϱRed − ϱNIR) were useful for monitoring vegetation (Payero *et al.*, 2004). Later, many other indices like the NDVI were developed from the simple ratio. A lot of green vegetation structural properties (e.g. leaf area index (LAI) and crown coverage), were found to greatly correspond with these vegetation index (VI) values (Purevdorj *et al.*, 2010). This therefore, inspires several other studies to try correlating vegetation indices to several ground cover parameters.

Merits and demerits of some vegetation indices (VIs)

The NDVI proposed by Rouse et al, (1974) is the most common and known vegetation index (VI) (Jensen, 2005). Its popularity is due mostly to its ability to eliminate topographic effects and viewing aspect, varying illumination conditions, and other atmospheric elements such as haze (Serban, 2011). Furthermore, the NDVI has normal distribution; in contrast to its predecessor the Simple Ratio (Mróz and Sobieraj,

2004). This makes NDVI very useful for global vegetation monitoring (Serban, 2011). Nonetheless, the NDVI is exposed to external influences unconnected to forest canopy (Gamon *et al.*, 2004; Peterson, 1991, as cited in Beck, et al. (2006)) and also it saturates over high biomes (Huete, 1998). This saturation effect was studied by Holben *et al.* (1980) and it revealed that the asymptotic nature of the relationship of the NDVI to biophysical properties limits its usefulness for high density vegetation conditions. Jackson *et al.*, (1983), also confirmed this by reporting that NDVI was most sensitive to vegetation early in the season - when influenced by soil background - and above 80% of vegetation cover, its sensitivity to vegetation dynamics reduced – saturation effect. The NDVI is defined by the equation found in table 4: The value of this index ranges from -1 to 1, and the common range for green vegetation is from 0.2 to 0.8 *(ENVI 4.7 help).*

The Enhanced Vegetation Index (EVI) and Atmospherically Resistant Vegetation Index (ARVI) form part of another group of indices which inculcates the blue band of remote sensing image to overcome the challenges of aerosol effects. Epiphanio and Huete (1995) assessed the bearing of sensor view and solar zenith angles on the NDVI, and concluded that variations in view angle could produce index fluctuations; therefore they came out with the ARVI. The Atmospherically Resistant Vegetation Index (ARVI) is an enhancement on the NDVI, it is found to be relatively resistant to atmospheric factors (for example, aerosol). It comprised amendments for molecular scattering and ozone absorption and also a function to correct the radiance in the red channel and stabilize the index to temporal and spatial variations in atmospheric aerosol content. It is most useful in regions of high atmospheric aerosol content, including tropical regions contaminated by soot from slash- and-burn agriculture.

Another VI that improves the quality of the NDVI product is the Enhanced Vegetation Index (EVI). This algorithm like the ARVI comprises of the blue reflectance as well to correct for soil ground cover reflections and lessens atmospheric influences, including aerosol scattering (Huete, *et al.*, 1997). The EVI does not saturate easily when viewing dense vegetation land covers. These characteristics altogether make it extra sensitive to differences in heavily vegetated areas. The value of the ARVI and EVI range from -1 to 1 and the common range for green vegetation is 0.2 to 0.8 *(ENVI help).* The MODIS Science Team is preparing the NDVI and EVI data product for global land cover monitoring.

1.1.3. Hypertemporal Image analysis

Hyperspectral image classification is analogous to Hypertemporal image classification. This is by the reason that, Hyperspectral image classification procedures hypothesize that different features of interest on the ground show reflectance spectra as varying by wavelength in predictable and differentiable ways, whereas, a Hypertemporal image profile of features exhibit predictable variation seasonally and even inter-annually (Knight *et al.*, 2006). In the instance of the latter, NDVI temporal profiles of healthy deciduous forests show high NDVI in the wet season as new leaves are formed and low NDVI in the dry season as leaves are shed. In the same manner, varying profiles of the same feature for different years could mean a change in the nature of the feature. This is therefore applied in mapping and monitoring land cover/vegetation through the periodical composited multi-temporal images collection and analysis over a year or more (Colditz *et al.*, 2006; Huete*, et al.*, 2002), to provide information on land cover/vegetation types as well as their trends resulting from seasonal and/or annual changes (Udelhoven, *et al.*, 2009: Neteler, 2005). Many studies explored the use of multi-temporal images taken within and across years to monitor ecosystems, map land-

cover/use, and detect changes, (Coppin *et al.*, 2004). These studies mainly engaged threshold-based methods, for instance, composting-algorithms, or Fourier series approximation to derive time-profile-based from large hyper-temporal datasets (de Bie, *et al.*, 2008). However, a new approach developed by de Bie, *et al.*, (2008), employs both spectral and temporal dimensionality of periodically composited vegetation index (VI) images for mapping and monitoring resources.

This approach involves two main stages; firstly, the selection of optimal number of classes and secondly, applying that number to classify the stacked multi-temporal vegetation indices to give a landcover map. This best number of classes for each stacked VI to be used for the classification is determined based on the estimations of optimal seperabilities per class. This is achieved using Erdas Imagine ISODATA clustering algorithm to classify the stacked multi-temporal VI images into series of numbers of classes, and the generated signatures evaluated in Erdas Imagine *Signature Editor*. The *minimum-* and *average-divergence* statistics are determined and plotted against corresponding numbers of classes to establish the ideal one required for the images' classification. The chosen classified map (based on the optimal classes number) is reclassified using a supervised approach which involves visual comparisons of the time-profiles generated from its signature file. This approach has been applied in several studies, for instance, in mapping gradient boundaries (Scarrott, 2009; de Bie, *et al.*, 2008), mapping ecology and relating it to landscape map (Ali, 2009), and extracting seasonality parameters that characterizes the to-and-from key dry and wet season grazing areas of pastoralist migrations in Kenya (Mulianga, 2009). In other studies, it was used to detect changes in natural resource states (Beltran-Abaunza, 2009), and to map and monitor crops and floods (de Bie, *et al.*, 2008).

In this study, the Hypertemporal analysis described above was applied to stacked Hypertemporal MODIS EVI and NDVI spanning the period of 2002 – 2010 with the aim of producing output cover maps for each index. These resulting cover maps for the indices under investigation were further analyzed statistically to establish the index that gives the better classification output to be employed in *C*-factor modeling.

1.2 Problem Statement

The Bosumtwi landscape has seen increases in farming activities and indiscriminate infrastructural expansions which are recently affecting the biophysical environment of the area. The former is due basically to the increases in population of the village dwellers as well as the shift from fishing to farming for subsistence; and the latter is mainly due to the expanding tourist industry. The vegetation cover in the accessible parts of the basin have become patchy due to the above mentioned anthropogenic activities leading to deforestation and subsequently, washing away of the topsoil. Erosion has become widespread in the basin leading to damage to roads and buildings. In order to estimate the erosion hazard of this catchment area using USLE, there is need of determining the Cover and Management (*C)* –factor.

The Normalized Difference Vegetation Index (NDVI) has often been used in estimating the *C* –factor, despite documented problems associated with this index and the proposals for several replacements believed to overcome most of difficulties associated with the NDVI's use. This study therefore, compared two VIs; the NDVI and the Enhanced Vegetation Index (EVI) by their ability to develop landcover maps for the study area and choose the better index of the two to develop a *C* –factor model for erosion assessment of the basin. Recent studies have used stacked Hypertemporal vegetation indices (VIs) to map and monitor vegetation by the use of temporal profiles corresponding to landcover classes. Also in this study, the temporal aspects of the

various landcover types were investigated to establish which number of classes of each stacked multitemporal vegetation index that could be applied in classifying them.

1.3 Research Objectives

The main objective of this study was to map cover types using ASTER and MODIS in Bosumtwi basin by investigating the temporal properties of MODIS Hypertemporal vegetation index, and applying the better index for USLE's *C* - factor estimation for the basin.

1.4. Specific Objectives

The research scope also involves the following specific objectives to be accomplished.

a. To Map Bosumtwi basin with high accuracy using ASTER image, and time-series MODIS NDVI and EVI. (This research employed an iterative approach of unsupervised classification of the MODIS time-series vegetation indices (VIs) data through an ISODATA clustering technique).

b. Compare the MODIS NDVI and EVI derived VI profiles and maps to select the better index for *C* – factor estimation of the basin.

c. Compare predicted map to real *C* – factor values of the better index. (The exponential function derived *C* – factor model was related to validation map consisting of literature *C* - factor values assigned to the classification map).

1.5 Research questions

1. Can the distribution of landcover types in the basin be mapped with high accuracy using:

    a) ASTER image and

b) MODIS derived vegetation indices?

2. Which index can be applied to better estimate *C* – factor of the basin?

3. How related are the predicted *C*-factor values to reality?

2.0. METHODOLOGY

2.1. Description of study area

2.1.1 Site selection

The selection of study area which is a pre-requisite for the research activities was done based on several criteria:

1. The study area should have natural forest, where forest conversion to other cover types is prevalent,
2. It should be a watershed research area, where anthropogenic activities are the main causes of soil erosion,
3. The study area should have recent time series remote sensing data, maps and other secondary data available for use in this study.
4. The study area should be accessible by foot, bicycle and by car.

2.1.2 Location, Climate and Land use/ Land cover types and Farming practices

The study area is the northern half of Lake Bosumtwi basin, about 19.5 square kilometers in area. Lake Bosumtwi is a natural lake formed from meteorite impart. It is located near the regional capital of Kumasi, which is also the second largest city in Ghana as well as being the capital of the Ashanti kingdom and Ashanti region simultaneously. The studies took place in the upper half of the Bosumtwi watershed, it extends from 6°33' 27.31" to 6° 30' 8.23" N and 1° 27' 13.3" to 1°21'34.1"W. The southern part was excluded due to inaccessibility to those parts. The Bosumtwi structure is centered at 06° 32'N and 01° 25'W was found to be of 1.07 million geological years. It is of scientific importance and many studies have been carried out there. For instance there are published works on the lake level, lake chemistry,

climate, and vegetation history through core studies (Koerberl & Reimold, 2005). The high-flying crater rim is elevated by 210 – 350 m above the lake level which also is about 80 to 100 m below the outside terrain of the basin (Koerberl & Reimold, 2005). Lake Bosumtwi is a closed-basin lake with a present-day area of 52km² and maximum depth of 78m.

Rainfall at Bosumtwi is lowest in January (average 17.0 mm) and highest in June (average 233.9 mm), and is highly variable from year to year. The Lake is hydrologically closed presently, with its water balance being dominated by rainfall on the Lake Surface and direct evaporation. Groundwater sources are negligible. Lake Bosumtwi lies in the path of the seasonal migration of the intertropical Convergence Zone (ITCZ), the atmospheric boundary between north-easterly continental trade winds and onshore south-easterly trade winds (Koerberl & Reimold, 2005).

The region around Lake Bosumtwi is widely covered by very dense, tropical rainforest. Where less dense vegetation is observed, this frequently represents patches of agricultural activity (Koerberl & Reimold, 2005). Mostly these are the accessible parts along the undulating basin of the lake. Cocoa plantations cover a significant area in the environs and on top of the crater's rim.

The dwellers in the twenty–two communities of Bosumtwi basin are fishermen and subsistence farmers (Boamah & Koeberl, 2007). They produce crops like plantain, cocoa, yam, cassava and vegetables; plantain being the commonest. Some of the fishes found are: *Tilapia discolour* (Kaabre), *Hemichromis faciatus* (Komfoo), *Saratheroden mutifaciatus* (Apatefufo) and *Tilapia bosmana* (Papari). Recently, the fishes are reducing in size (Konadu, 2004; as cited in Prakash *et al.*, 2005) and stocks have drastically reduced due to the use of unapproved nets and human population increase

(Dassah and Agbo, 2003 as cited in Prakash *et al.*, 2005), resulting in a shift to crop cultivation to support their income (Ofosu, 2006). Orthodox agricultural practices like shifting cultivation and slash and burn are applied by the farmers in the communities, (Prakash *et al.*, 2005). These subsistence activities and indiscriminate infrastructural development: attracted by the increasing tourist industry in the area: have been observed to be quickly changing the forest landscape of the basin (Boamah & Koeberl, 2007). These activities remove the vegetation cover of the soil leading to soil erosion by rainfall.

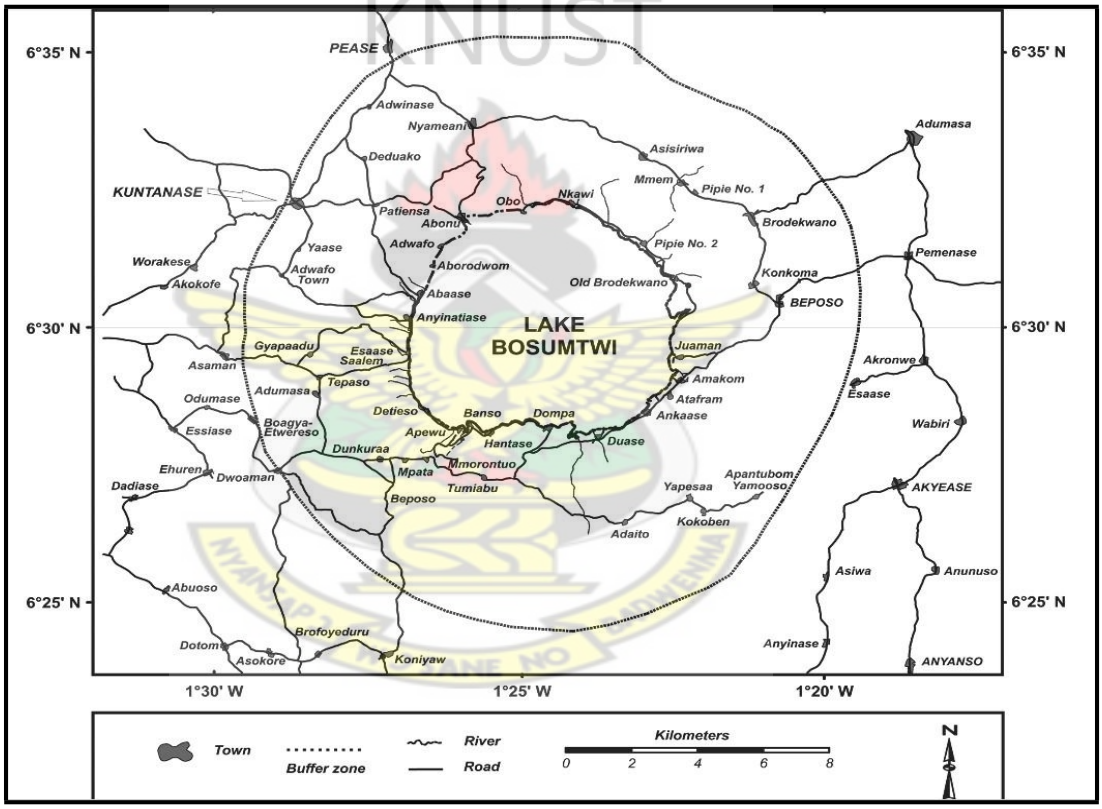

Figure 2: A map extract showing the near and far surrounding communities of Bosumtwi Lake (Adopted from Boamah & Koeberl, 2007)

Erosion is widespread in the area; causing top soils to be washed to the foot of the basin which ultimately has become adopted ground for cheaper and productive farming (Ofosu, 2006). The detriment is the damage done to road facilities, making

them unmotorable. Erosion, bush burning and felling down of trees are believed to have destroyed known habitats of certain creatures like monkeys, butterflies, African parrots, pigmy crocodiles and a lot more (Ofosu, 2006). Erosion indicators observed are of varying forms; they range from sheet and rill erosion to mass movement of soil, forming gullies and badlands, which are common sights across the catchment area.

STUDY AREA: UPPER HALF OF BOSUMTWI BASIN

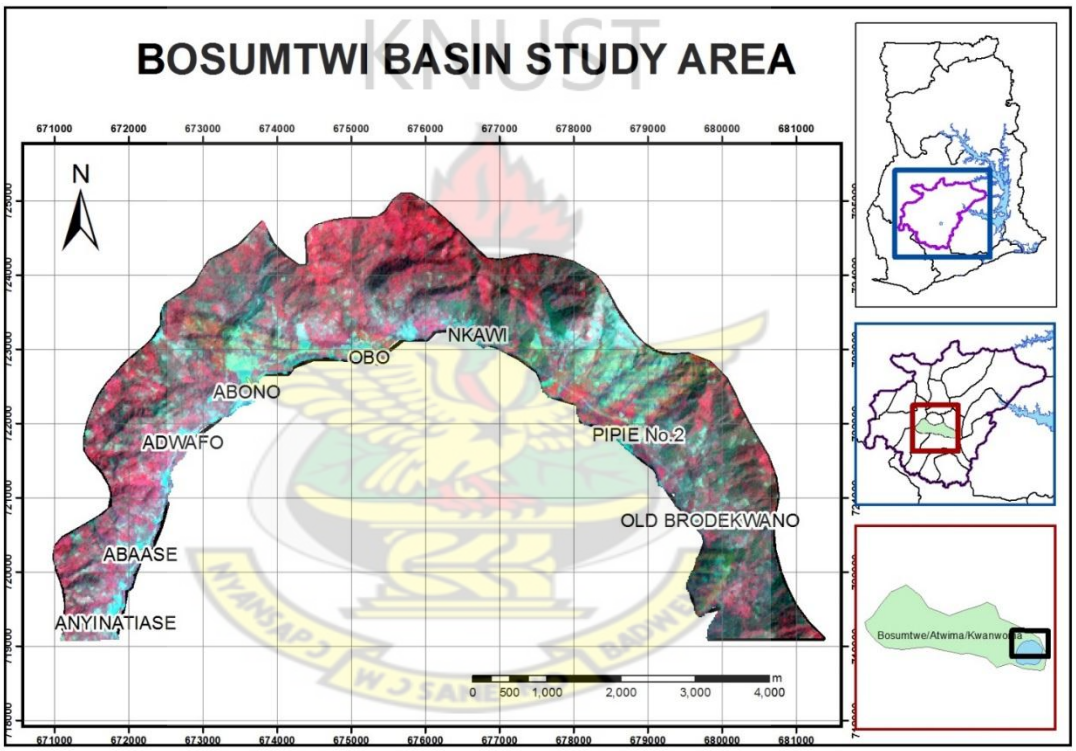

Figure 3: False color composite (FCC) of the study area as observed by the ASTER sensor. The Lake body is shown in blue.

2.2. Description of data used

Vegetation index values change periodically, Gitas, *et al.*, (2009) therefore a high temporal resolution satellite image is needed to estimate the *C*-factor periodically. Currently, the use of NOAA – AVHRR, MODIS, and SPOT – Vegetation data; - with spatial resolutions ranging from 250m to 7km and at most at a 10-daily availability of products - provide the option to study and obtain insights to temporal dynamics due to their global high revisiting frequencies (de Bie, *et al.*, 2008). The *terra* and *aqua* Moderate Resolution Imaging Spectroradiometer (MODIS) satellite data was used in this study. This MODIS package consist of high quality 250m resolution NDVI and EVI data of both *aqua* and *terra* (MOD13Q1 and MYD13Q1) satellite, they altogether provided an 8-day composite data for the analysis. There are two vegetation index (VI) algorithms for MODIS land products. The standard normalized vegetation index (NDVI) described as the "continuity index" to the existing NOAA-AVHRR derived NDVI and the enhanced vegetation index (EVI). During the launch of the terra-MODIS, there was almost a 20-year NDVI global data set (1981 – 1999) from the NOAA – AVHRR series, which is extended by MODIS data to offer a long term data record for use in monitoring studies. The EVI provides improved sensitivity to changes in vegetation from sparse to dense vegetation conditions. These two indices are complimentary in global vegetation studies and advances upon the extraction of canopy biophysical parameters (Huete *et al.*, 1999). Despite the low spatial resolution of the MODIS image, the high temporal resolution compensates for and helps detect dynamic processes in the biosphere (Udelhoven, *et al.*, 2009). Time profiles generated from MODIS and other hyper-temporal data has proven useful in phenological modifications studies (de Bie, *et al.*, 2008; Khan, 2011; Scarrott, 2009; Ali,

2009; Mulianga, 2009; Beltran-Abaunza, 2009). The *Terra* and *Aqua* MODIS (MOD13Q1 & MYD13Q1) satellite data used in this study altogether provided an 8-day composite data for the analysis.

The Advanced Spaceborne Thermal Emission and Reflection Radiometer (ASTER) was used to develop a baseline cover map which was used for validating the NDVI and EVI cover maps. Both ASTER and MODIS sensors are onboard Terra satellite, they are optical sensors that can observe the wavelength range from visible to thermal, and these sensors have the possibilities of simultaneous observation (Yamaguchi *et al.*, 1998). The ASTER is a multispectral sensor consisting of devices covering three different spectral ranges. These are three (3) bands of 15m resolution visible/near infrared (VNIR) sensor covering green, red, and near infrared wavelengths. It also consists of 30m spatial resolution sensor with 6 bands that cover shortwave infrared wavelengths with one nonfunctioning. Thirdly, onboard also is the thermal infrared sensor that covers 5 bands at a 90m spatial resolution.

Table 1: The secondary data used for the study and their sources.

Secondary data	Year	Source
ASTER satellite image	2010	ITC
MODIS satellite images	2002 - 2010	http://earthexplorer.usgs.gov
Topographic map (1:50000)	2005	ITC database
Digitized contour map (1:50000)		KNUST

The boundary shapefile of the study area was digitized from a georeferenced topographical map. This area (below) consists of the northern part of the watershed.

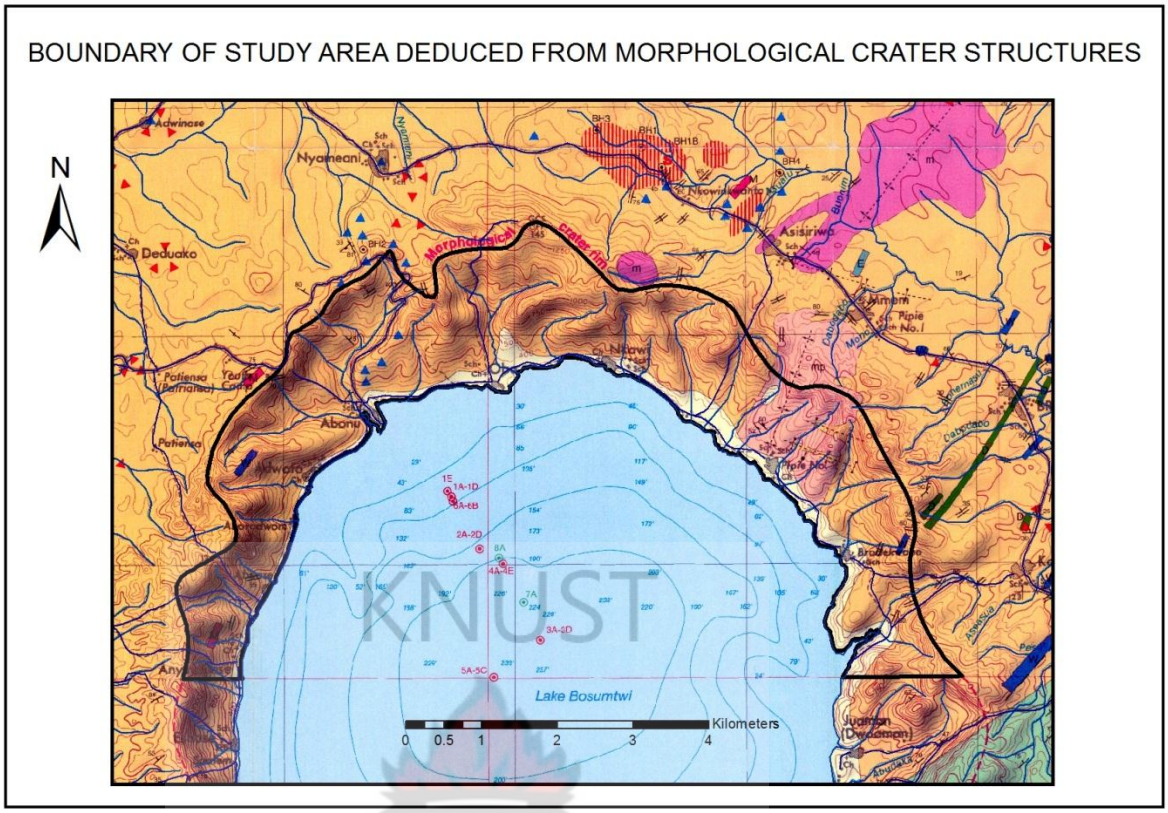

Figure 4: The study area shown as thick dark polyline on a topographic map, located on the northern half of the basin. It lies between the lake shore and the morphological crater rim.

2.3. Materials

2.3.1. Software

Table 2: Software used for the study

Software	Used for
ERDAS Imagine	Land cover map preparations, MODIS data preparations and classifications.
MRT	Sub-setting and reprojection of MODIS data
ArcGIS 10	Database creation and geospatial analysis
MS Excel	Data entering and statistical analysis
MS Word,	Word processing
MS Visio	Flowcharts

2.3.2. Instruments

Table 3: Instrument used for the fieldwork

Instrument	**Used for**
Ipaq with GPS	Navigation and location of sample plots, and handheld GPS
Measuring tapes	Distance measurements
Clinometers	Slope determination
Densiometer	Canopy cover measurement
Digital camera	Photographs of study area and fieldwork

2.4. Flow chart

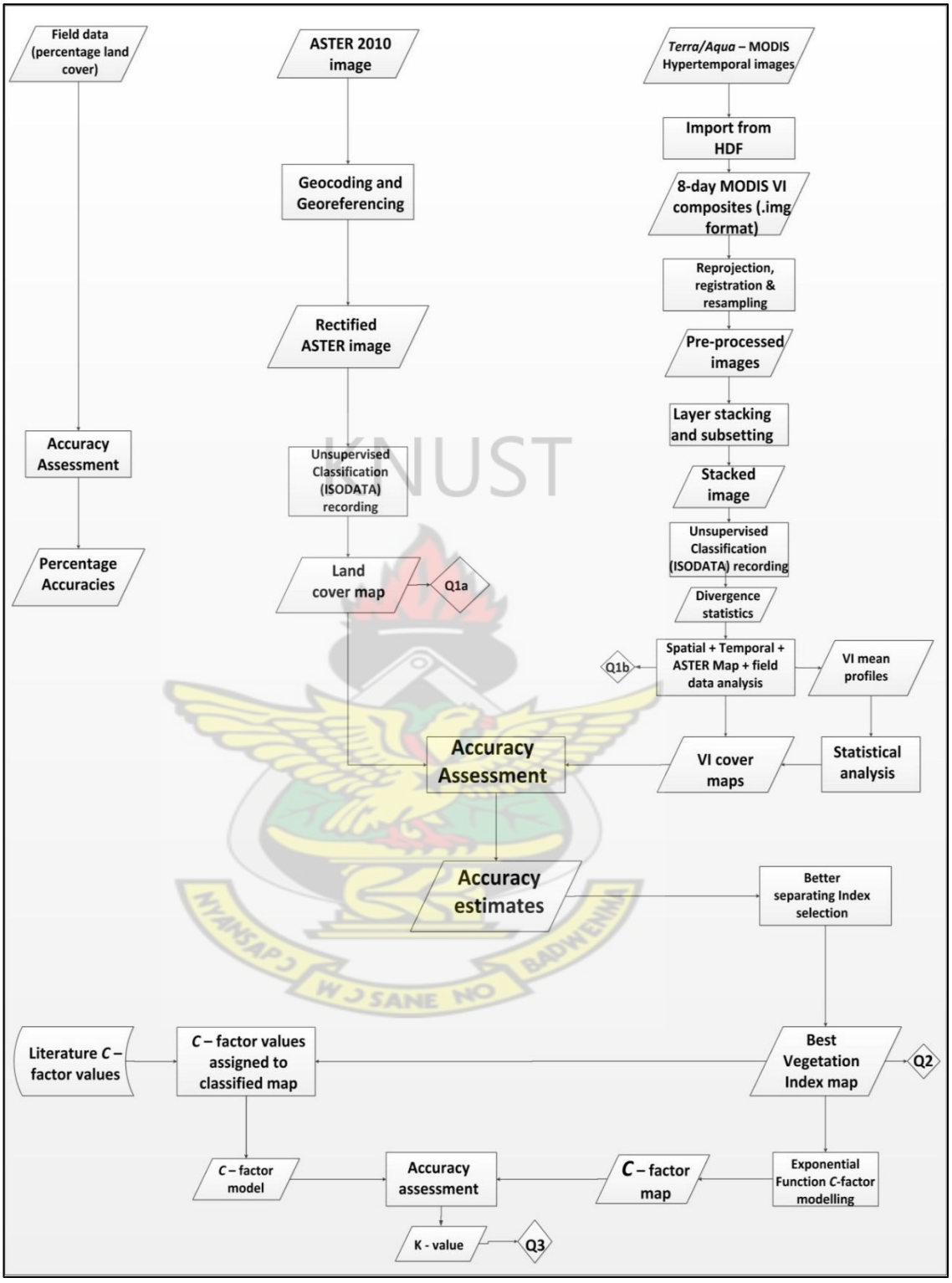

Figure 5: Flowchart of the study

2.5. Research methodology

This study was conducted in four (4) main methodological steps:

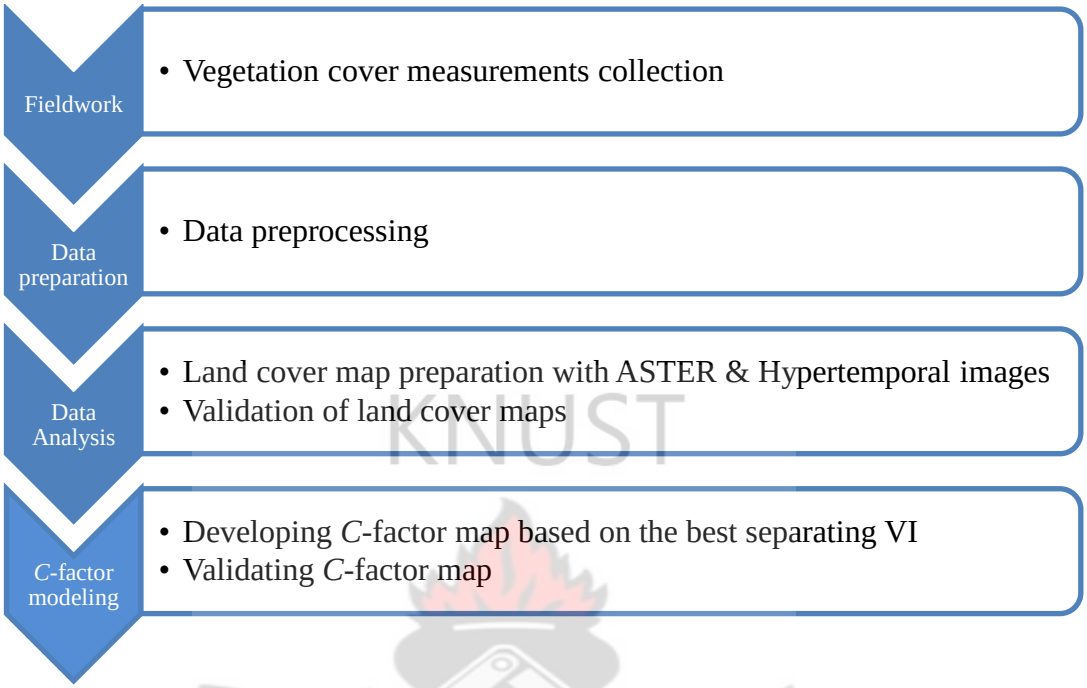

Figure 6: Methodological steps

2.6. Data preparation: (ASTER and MODIS)

The two sets of satellite data were preprocessed, the ASTER used to map the study area based on ground truth data, and the MODIS time-series data also analyzed spatially and temporally before using it to map land-cover and the *C*-factor.

2.6.1 Georeferencing

A georeferenced ASTER image; dated February, 2010, was used to develop a land cover map of the study area. A Geometric correction and georeferencing of the ASTER image were based on the World Geodetic System '84 (WGS 84/UTM) projection system, this was carried out by selecting appropriate number of well recognized ground control points (GCPs), thus, road and river intersections. These

GCPs were also collected in addition to cover measurements during the fieldwork. A 1st order polynomial transformation was used, in an effort to keep the Root Mean Square Error (RMSE) lower than 0.5 pixels (Lillesand *et al.*, 2004), and in this case an RMSE value of 6.3m was realized. The georeferencing was done in ArcGIS 10 software environment. The study area boundary shapefile was delineated from a topographical map and then used to subset the MODIS images using Erdas software.

The 16 days composite 250m terra- /aqua-MODIS data spanning the period between June 26th, 2002 and March 30th, 2010 were downloaded free of charge from the Global Landcover facility downloading site (http://earthexplorer.usgs.gov). The images are subsets of an original scene of tile (*h17v08*) and were originally in HDF format and Sinusoidal projection system projection. The selected images were reprojected for geometric correction with MODIS Re-projection Tool (MRT) and corrected to UTM zone 30 of Ghana and afterwards imported into Erdas Imagine software for extraction of vegetation indices and bands.

The stacked VI images were georeferenced using identifiable features such structures and shoreline based on the already georeferenced ASTER image and topographical map of the study area. A geographical sub-setting of the image to the defined Bosumtwi basin study area boundary was done as well in Erdas software.

2.6.2 Field sampling

Data of percentage canopy cover were collected through field measurements, based on stratified random sampling approach. The study commenced with field measurements of vegetation percentage cover in September and October, 2011. The stratification was based on an unsupervised classification; this was to randomly select fifty (40) plots each from the classes of forest, shrub, farm, bare and settlements cover

types. Point shapefiles were generated and then transferred unto the Ipaq, to aid in navigating to these positions.

The land use and land cover were recorded by observation and the vegetation percentage cover by field measurements. Densiometer was used to determine the percentage cover of the tree layer, and line transects sampling of shrub layer and grass layer. A reference location was chosen for each plot based on a dominant tree. Densiometer readings were recorded in the four (4) cardinal directions facing away from the reference positions at distances of 7 and 14 meters. The average vegetation cover is determined and recorded for the plot. For the farmlands and shrub classes, 20 meters line transects was used. Since the terrain is varying in slope, linear measurements were adjusted using clinometer readings.

2.6.3 Accuracy assessment of the ASTER land cover map

The land cover map product derived from unsupervised classification of the 2010 ASTER image was validated using data collected from the field. The parameters collected are landcover types and percentage vegetation cover of the vegetation classes. A total of 100 field validation plot measurements comprising of all classes under consideration were employed. An error matrix, from which statistics and indices that indicate the accuracy of individual classes and of the whole map was then derived from the classification.

2.7. Data analysis and Modeling

2.7.1. Vegetation indices algorithms

The available MODIS indices (NDVI and EVI), were downloaded from http://earthexplorer.usgs.gov, website. The formulas used to compute them are as follows:

Table 4: The algorithms of MODIS NDVI and EVI employed in the study.

	EQUATIONS	References
1	$NDVI = \frac{\rho NIR - \rho Red}{\rho NIR + \rho Red}$	Rouse, 1973; Fassnacht *et al.*, 1997; Smith *et al.*, 1991.
2	$EVI = 2\frac{\rho NIR - \rho Red}{\rho NIR + C_1 \times \rho Red - C_2 \times \rho Blue + L}$	Huete, *et al.*, 2002

Where ρNIR, $\rho Blue$ and ρRed are the surface reflectance in their respective sensor bands; L is a canopy background adjustment that addresses nonlinear differential NIR and red radiant transfer through a canopy. C_1 and C_2 are the coefficients of the aerosol term, which uses the blue band to correct for aerosols in the red band. The coefficients adopted in the MODIS EVI standard product are $L = 1$, $C_1 = 6$ and $C_2 = 7.5$

2.7.2. Multitemporal Vegetation Indices (VI) classification

The approach employed, involves two main stages; the selection of optimal number of classes and applying that number to classify the vegetation indices (VI). The best numbers of classes for each VI to be used for the classification were determined based on the estimations of optimal seperabilities per class. This was done using an approach developed by de Bie *et al.*, (2008) in Erdas Imagine software which employs ISODATA clustering algorithm to classify the images, thereafter the output signature files were evaluated to produce average and minimum seperabilities. As a first step, stacks of Hypertemporal *terra*- and *aqua*-MODIS VI images were compiled from June

26th, 2002 to March 30th, to give 358 images each for NDVI and EVI. Unsupervised classifications runs in Erdas Imagine were performed on the stacked VI images with pre-defined number of classes (4 – 30), increasing each preceding step by 1. The maximum number of iterations was set to 50 and the convergence threshold to 1.0 for each index, and for all 4 to 30 numbers of classes run. The maximum iterations control the output of the ISODATA by means of stopping the utility at a threshold while the convergence threshold is meant to prevent the ISODATA utility running indefinitely. The optimum number of classes that would best classify each VI data was determined based on the plots of the divergence test results. The divergence test measures the distances between divergence signatures for each number of classifications and determines the mean signature seperability. Two divergence statistics; average and minimum seperabilities were determined and plotted against the number of classes (these are shown in figure 11 and 12). The minimum separability denotes the similarity between the two most similar classes and the average separability also represents the similarity among all classes. In order to choose the best number of classes for each image, peaks were observed in both the average and minimum seperabilities for the indices. Both statistics should be high at the least number of classes for the NDVI, and EVI images to give the optimal number of classes for the respective classes. Different VIs gave different peaks in their respective plots, indicating the best numbers of classes that will best classify NDVI, and EVI, respectively.

The observed optimal numbers of each of the indices (derived from the divergence test) was used as inputs in selecting base maps for further analysis. The 21 NDVI and 20 EVI classes' maps were selected and by supervised grouping of their respective temporal-profiles based on their characteristics using both visual assessment and dendrograms classes. Another supervised classification was done This was done by

finding the mean statistics of the signature files (generated by unsupervised classification of the VIs based on the chosen class numbers) column-wise which represents a point in the time-series data in *Erdas Signature Editor*. The index values by class of each point in the time-series data were then exported as text file from Erdas to excel. The mean values were computed by arranging yearly column values by class in a separate row to produce profiles of the respective classes' maps. Several of the mean profile values were grouped together based on their similarities and area adjacency to produce the baseline maps of the respective indices for further analysis. Two output profile groups are shown in figure 7 and 8, the rest can be found in appendix 3. The grouping of mean annual profiles is further elaborated in the next section.

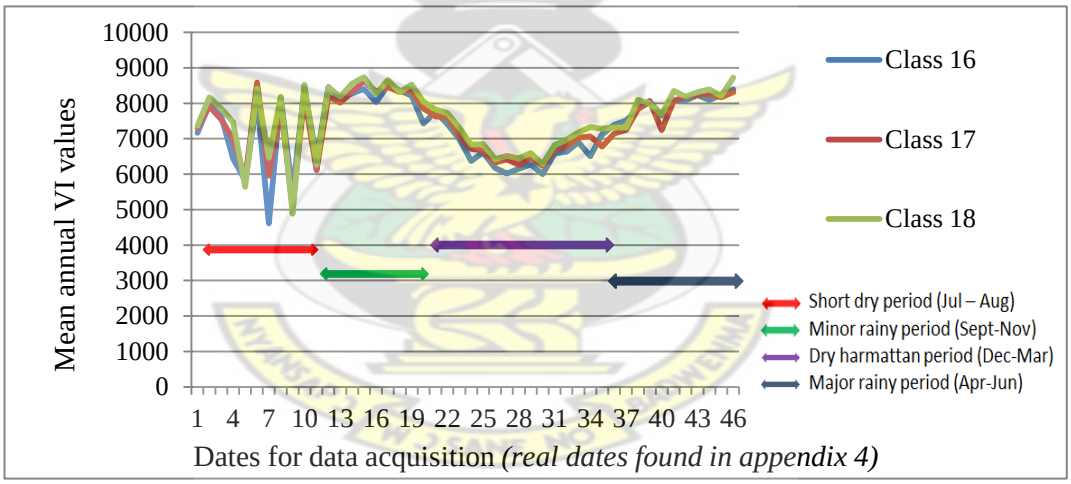

Figure 7: Profile group representing shrub and farmland on NDVI classification map.

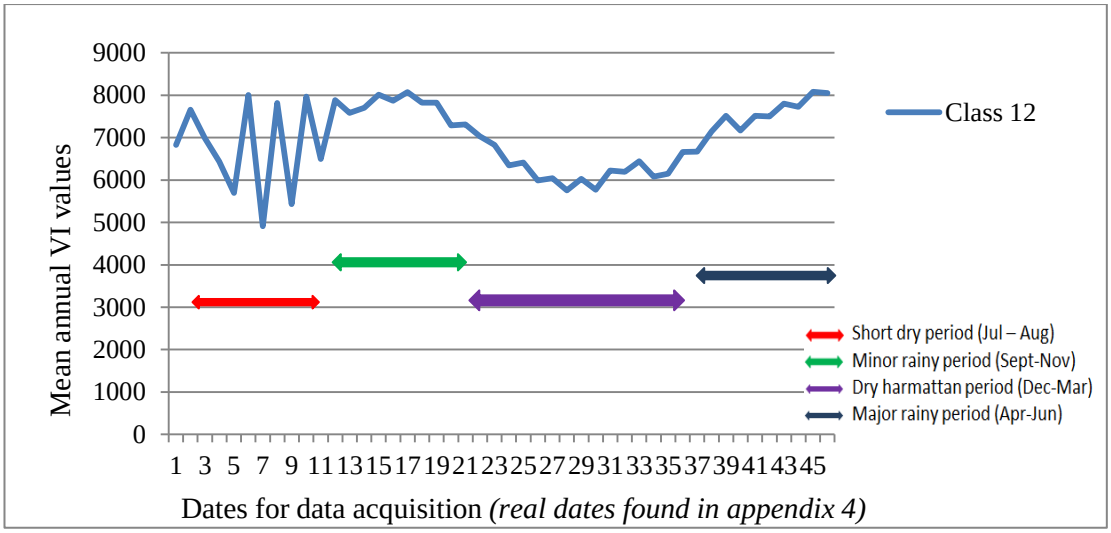

Figure 8: Profile group representing Bare/grassland on NDVI classification map.

2.7.3. Supervised classification of MODIS VI maps and legends matching using ASTER landcover map.

In the second stage of the approach, the VI output maps were reclassified and compared with ASTER landcover map to assign legends to the identified classes. The unsupervised classification was followed by a supervised classification; this involves merging classes based on similar signature files to generate more representative maps. The generated mean VI profiles revealed similarity/dissimilarity in them based on the temporal behavioural patterns of the images. Using these patterns in combination with dendrogram tool of SPSS, groupings were done, putting into consideration the area weights (thus, in such a manner that areas represented by them were usually adjacent to one another). An example is illustrated in figure 9. The cover maps derived from MODIS Hypertemporal VI images were compared with the reference cover map to allocate classes to the classes formed. This was undertaken by using the geo-link utility in Erdas Imagine, to visually compare the dominant class as shown on the ASTER map to the representative area on the VI maps (classified according to the profile groups).

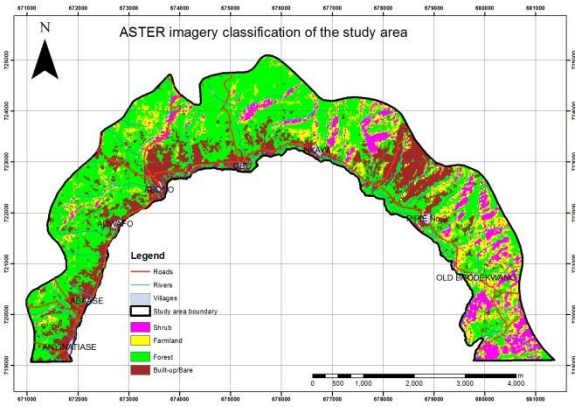

ASTER imagery classification map

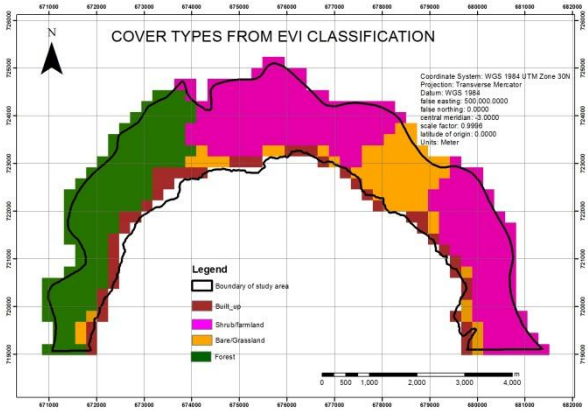

EVI classified map showing Shrub/farmland unit in pink

Figure 9: The ASTER land cover map compared to VI map to identify cover classes

2.7.4. Accuracy assessment using ASTER landcover map

This final *VI* maps were validated with the existing validated landcover map (the ASTER classification map, validated with ground truth data), to derive quantified data on the land cover types indicated by each *VI* classes. One hundred and fifty (150) random sample points were generated from the ASTER map and their corresponding cover classes were recorded. The accuracy assessment utility of Erdas Imagine was used to assess the accuracy of the *NDVI* and *EVI* classified maps with the 150 validation points collected from the ASTER map. The Kappa coefficients of the two assessments were compared, to choose the classified map that is closer to prevailing ground conditions. The Kappa coefficient states the proportionate reduction in error produced by a classification process compared with the error of a completely random classification. For instance, a kappa value of 0.82 infers the classification is avoiding 82% of the error that a completely random classification generates (Congalton, 1991).

2.7.5. Estimating the USLE-*C* - factor map from best vegetation index

The Vegetation index that best distinguishes between land cover types was applied in estimating the C- factor model. The two main methods employed to convert index images to C – factor values are: the linear least square method (LLS) (de Jong, 1994) and the exponential function (Van der Knijff *et al.*, 1999).

The C-factor map according to the LLS is done based on the assumption that: on the C-factor scale of 0 to 1, bare areas have C-factor values of 1 and highly dense vegetated areas, values of 0. Therefore a least-square regression was fit using vegetation index as the independent variable and plot measurements of C-factor (of bare and vegetated areas) as the dependent variable to extrapolate C-factor for each of the remaining pixels of the image. This results in a spatial data layer of C factor, an input for the USLE model.

The second approach, the exponential function (EF) method was based on several experiments and is believed to be an improvement on the linear least square approach. The (EF) model is shown below:

$$C = \exp\left(-\alpha\left(\frac{VI}{\beta - VI}\right)\right)$$

Where: α, β are parameters that determine the shape of the VI-C curve. The value α = 2 and β = 1 are mostly used.

Based on the above stated formula of the exponential function, *C*-factor images were calculated using 2010 MODIS data in Erdas Imagine software. Vegetation index varies seasonally as shown by the temporal profiles; therefore periodical *C*-factor models were developed for the four different seasons observed every year in southern Ghana. Erdas modeler tool was used for the conversion of images into index values range (i.e. -1 to +1), and after the final conversion of VI values into *C*-

factor maps. The seasonal C-maps for the study area were created following a four-step procedure.

a) The E. F. above was used to convert pixel-by-pixel estimates of EVI to *C* – values.

b) The 8-daily *C* – maps are aggregated into seasonal images by taking, for each pixel, the average *C* – value for all succeeding images within the periods of April – June, July – August, September - November and December – March.

c) This was followed by aggregating the four seasonal *C* – maps into an annual *C* – map.

d) For the four cover classes observed on the EVI classified map, range of *C* – factor values were obtained.

2.2.6. C-factor map validation

To validate the outputs derived from NDVI based *C*-factor maps, there is need for reference data and the approach used often when field collected validation data are unavailable is to compare the results with *C*-factor model developed from cover map and literature assigned values (Suriyapat & Erencin, 2000). The resulting map of the unsupervised and supervised classification of the best vegetation index image was used for validation. The *C* - factor values allocated for the different cover units were derived from literature. The *C* - factor values for the same land cover types vary geographically, therefore values taken came from researches done in Ghana (Table 3: is a summary of the *C* – values used). These values are collections of research results from many authors as cited in (Mati and Veihe 2001).

Table 5: Literature cited *C* - factor values

Land Cover Class	*C*-factor	Location
Bare	1	Ghana
built-up	1	Ghana
Forest	0.001	Ghana
Farm	0.2 – 0.3	Ghana
Shrub	0.1 – 0.3	Ghana

The steps followed to validate the annual *C* – factor map is as follows:

a) Codes representing *C* – factor values obtained from literature were assigned to the EVI classes' map. The built – up and bare cover classes for EVI were merged so as to have same classes as the reference map.

b) Random points were generated and used to extract *C* – value codes from the ASTER cover map and annual *C* – maps, respectively.

c) Accuracy assessment tool in Erdas Imagine was used to validate the *C* – factor map with literature values as references.

2.2.7 Comparing *C*-factor maps to VI land cover map

Since no *C*-factor validation data were collected on the field due to limited time for fieldwork, the exponential function (E.F) derived *C*-factor map was compared with the landcover *C*-factor map (made of literature *C*-factor values assigned to the cover classes on the EVI map). This was achieved by reclassifying the *C*-factor map into 6 classes and merging it with digitized classes on the EVI map using *Union Function* in ArcGIS 10 (see *appendix 5*). The *C*-factor distribution for class was then computed.

3.0. RESULTS AND ANALYSIS

3.1. Vegetation mapping using ASTER image

The land cover in the study area was classified into 4 classes based on Maximum Likelihood classifier: The land cover classes analyzed in this work are the dominant cover types found in the basin. An unsupervised classification was performed in order to differentiate the main land cover types in the study area. The cover map were validated based on sample tests collected on the field, they are; forest, bare/built up, farms, and shrubs. These are elaborated in the table: (6) below. The classified land-use/cover map of north Bosumtwi basin is shown in figure 10. An accuracy assessment result of 84.5% was realized. This map produced formed the basis for the latter analysis in this study. Forest dominates the landscape with about 1,000 ha area, followed by built – up/bare cover types (400 ha), farmlands (370 ha) and lastly, shrub (200ha). This is illustrated in figure 11.

Table 6: Description of the main land-use/cover types in the study area

Land-use/ cover type	**Description**
Shrub	Areas farmed in the past and left to recover, or areas of steep terrain without tall trees. It is made up of thickets of shrubs and trees ranging from 2m to about 15m.
Farmland	These are lands put under any kind of cultivation, for instance annual mixed cropping, perennial farms, cocoa and oil palm plantations
Forest	These are areas of high tree cover density (both open and

	closed canopy) reaching above 15m. They comprise of semi-deciduous forest patches found mostly up the basin.
Built-up/Bare	Areas with high intensity of infrastructure and exposed land areas resulting from natural or anthropogenic causes.

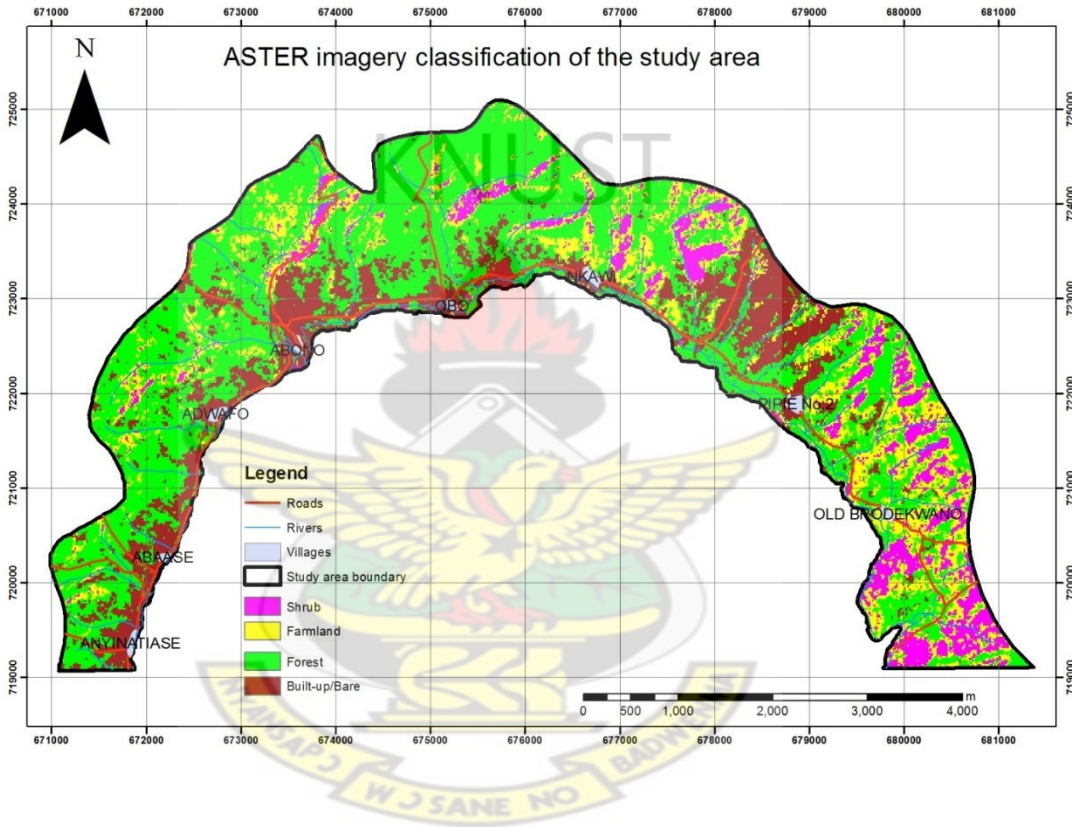

Figure 9: Classified land-use/cover map of portion of Bosumtwi basin.

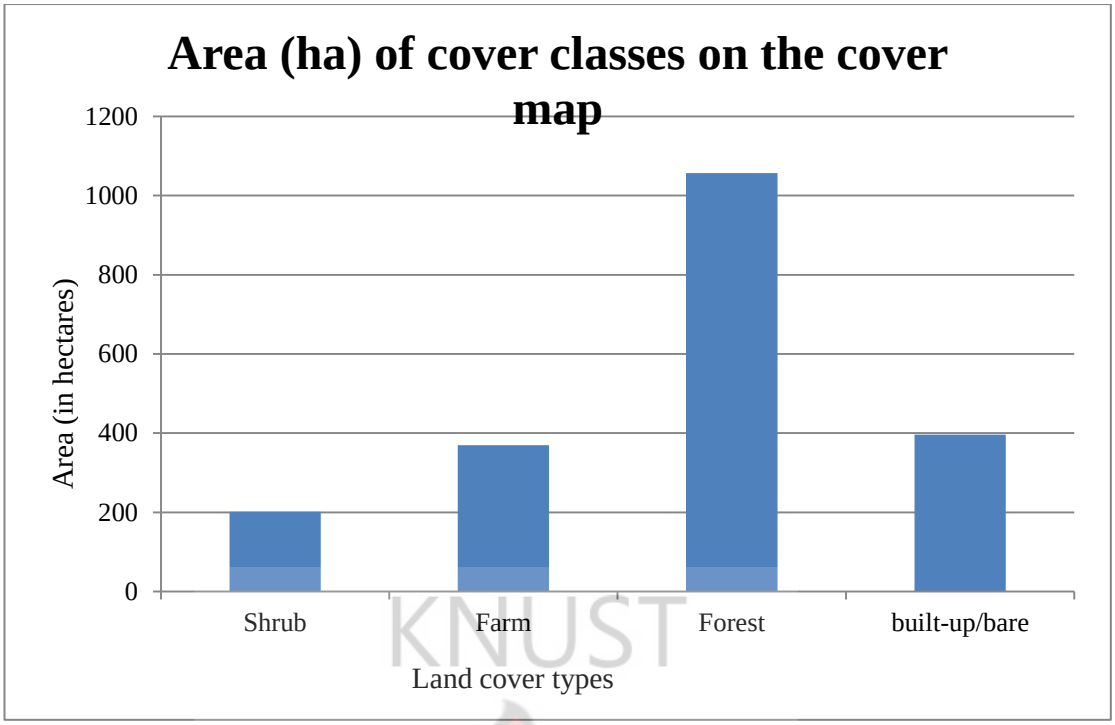

Figure 10: Classes distribution in the study area (ha)

3.2. Accuracy assessment of Landcover map using ASTER image of 2010

Hundred ground truth data were used for assessing the accuracy of the ASTER Landcover map of 2010. The result of the unsupervised classification confusion (error) matrix and accuracies are shown in Tables 7 and 8 respectively. Shrub and bare/built-up cover types recorded the highest producer accuracy percentage of 100; this was followed by forest with 72.2% and lastly, farmland with 53.9%. Built-up/bare cover type again recorded 100% users' accuracy, followed by shrub, forest, and farmland with 84.6%, 80% and 50%, respectively. The overall classification accuracy is 84.5% and overall kappa statistics is 0.7924.

Table 7: Classification error matrix of the ASTER landcover map

	Shrub	Farmland	Forest	Built up/ Bare	Total	Error of commission (%)
Shrub	**11**	0	2	0	**13**	15.4
Farmland	0	**7**	7	0	**14**	50
Forest	0	6	**24**	0	**30**	20
Built up/ Bare	0	0	0	**43**	**43**	0
Total	**11**	**13**	**33**	**43**	**100**	
Error of omission	0	46	27	0		

Table 8: Classification accuracies of the ASTER landcover map

Land cover class	Reference totals	Classified totals	Number correct	Producer accuracy (%)	User accuracy (%)	Kappa
Shrub	11	13	11	100	84.62	0.8278
Farmland	13	14	7	53.85	50.00	0.4278
Forest	33	30	23	72.72	80.00	0.7185
Built up/ Bare	43	43	43	100.00	100.00	1.0000
Total	100	100	87			

Overall Classification Accuracy = 84.47%

Overall Kappa Statistics = 0.7924

3.2. Multitemporal Vegetation Indices (VI) analysis

3.2.1. ISODATA classification

As described in the section 2.7.2., the approach involves two parts: firstly, the spectral separation of classes as was determined for the stacked multitemporal vegetation indices using divergence statistic (Swain and Davis, 1978; ERDAS IMAGINE, 2005), and secondly; analysing the base maps produced based on the optimal number of classes. Divergence statistical measures of distance (i.e. class seperabilities) of the 4 to 30 generated cluster signatures (Erdas, 2003) were employed to relate the classification outputs of the predefined classes. The optimal class numbers 21 and 20 representing NDVI, and EVI respectively were chosen to classify the respective images. The choice of this optimal number is dependent on whichever class indicates the first highest peak for either minimum seperability and/or average seperabilities. As can be observed in figures 12 and 13; the separability plots of average (coloured blue) and minimum (coloured red) seperabilities against their corresponding class numbers (on the horizontal axis), this aided the choice of best classification numbers. The observed highest peaks for both seperabilities in figure 12 representing NDVI occurs for class 21 with average and minimum seperabilities values of 603 and 17. Beyond Class 21, the average separability values for the later classes reduced and became normal. And also, the highest value recorded for the minimum separability was 17 for Class 16, and remains constant for the rest of the classes. The same manner of analysis performed on the EVI data presented the graph as shown in figure 13. The minimum seperability recorded the highest value of 17 for Class 15 and then reduced 10 for Class 16, after which it increased slightly to 11 for Class 19 and afterwards maintained the same value for all the other higher classes. Unlike the minimum seperability, the maximum seperability produced the highest value of 1035 for Class 20 and reduced to 790 for

the next class and rise gently for all the higher class numbers. From these observations as displayed by the graphs and the recommendation to select an optimal number higher than 20 (*personal communication*), the classes' numbers 21 and 20 were selected for the NDVI and EVI, in that order.

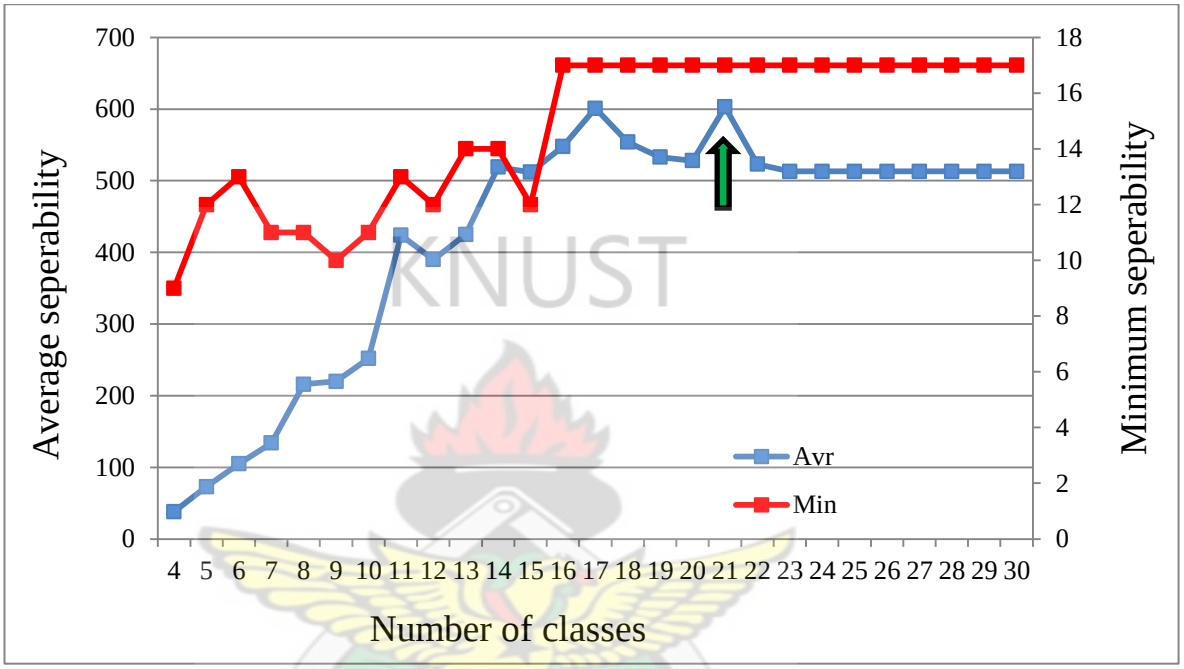

Figure 11: Plot of average (left *y-axis*) and minimum (right *y-axis*) seperabilities against the number of classes of NDVI (*x-axis*). The occurrence of a first peak for both seperabilities on the graph gives the best number of classes. The NDVI graph shows the first peak on class 21.

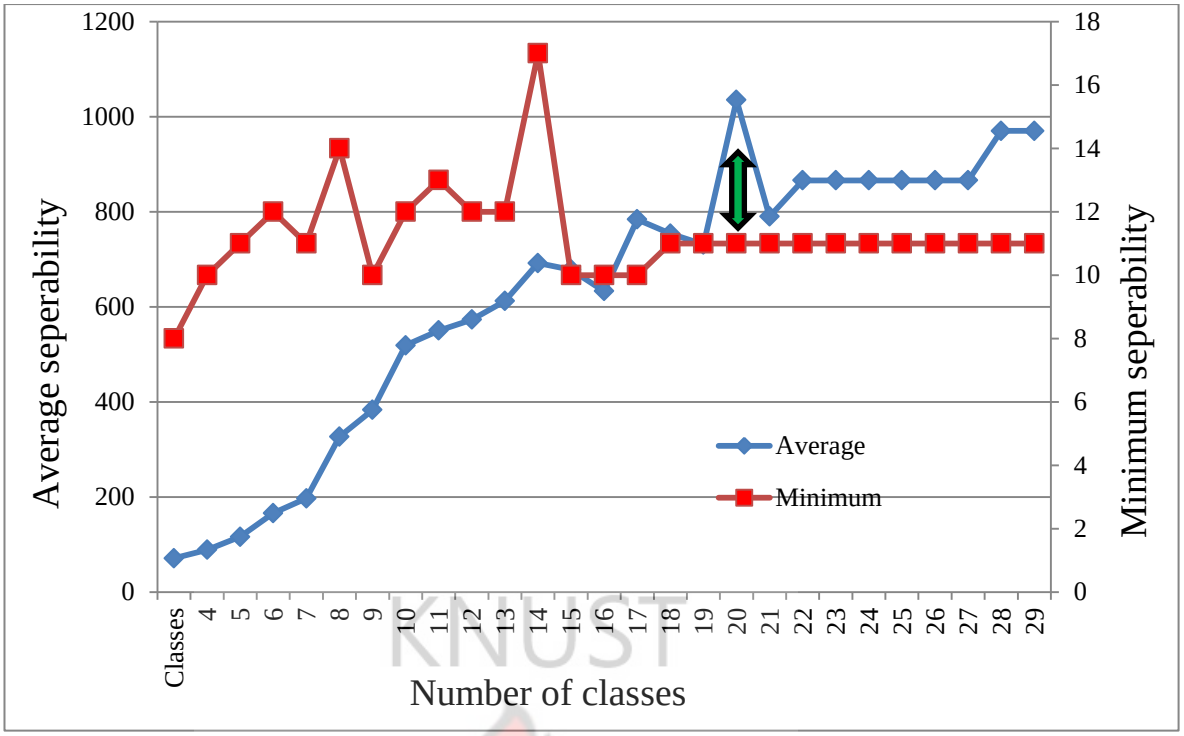

Figure 12: Plot of average (left *y-axis*) and minimum (right *y-axis*) seperabilities against the number of classes of EVI (*x-axis*). The occurrence of a first peak for both seperabilities on the graph gives the best number of classes. The EVI graph shows the first peak on class 20.

The second stage of this approach involved classifying the stacked Hypertemporal images based on the observed optimum classes' numbers and generating mean annual index values to be applied in supervised classifications of the resultant maps. The generated mean VI profiles revealed similarity/dissimilarity in them based on the temporal behavioural patterns of the images. Based on these patterns, they were grouped, putting into consideration the area weights (that is, in such a manner that areas represented by them were usually adjacent to one another). The SPSS dendrograms helped in classifying these class units into main classes (shown in *Appendix 2*). Four groups of VI profile units were observed in both the NDVI and EVI data. The Table 9 below shows the various profile groups identified for each VI image also *Appendix 3* consist the plots. The NDVI profiles 16, 17, and 18; formed

Group A, and the standalone profile 12, represents *Group B*. The other NDVI profiles 2, 4, 5, 6, 9; forms *Group C* and lastly, profiles 8, 9, 10, 11, 13, 14, 15; were assigned *Group D*. For the EVI supervised classification, profiles 8, 15, 16, 17 formed *Group A*, and profiles 8, 9, 10, represents *Group B*. Others are profiles 2, 3, 4, 5, 6, 7 made *Group C* and lastly, profiles 11, 12 and13 were assigned to *Group D*. The output maps from these supervised classifications are shown in figures 14 and 17, with their corresponding average profiles (or legends) illustrated in figures 15 and 18.

Table 9: Identified profile groups used from VI map supervised classification.

Profile groups	**NDVI groups**	**EVI groups**
A	16,17,18	14,15,16,17
B	12	8, 9, 10
C	2,4,5,6,9	2, 3, 4, 5, 6, 7
D	8, 9,10, 11, 13, 14,15	11, 12, 13

The reclassification of the VI map classes based on mean profile values representing four classes for each of the indices. The output maps with their profile legends are shown in figures 12 - 15. The area of the cover types on each of the VI maps are illustrated on figures 14 and 17. For both indices, the forest cover dominates the study area, followed by shrub/farmland cover, built-up and lastly, grassland.

3.2.2. VI legends matching with cover types.

The cover maps and their respective annual mean profiles *(Appendix 3)* derived from MODIS Hypertemporal VI images were compared with the reference cover map to

assign classes to the cover/profile groups. The cover map with an accuracy of 85% was developed from single-date ASTER image and field data, was used as the reference for allocating class names. The shrub and farmland classes were difficult to delineate on the MODIS maps unlike the ASTER map due to differing pixel resolutions and were therefore merged as one unit. The detail descriptions of the classes are as follows:

Group A: The shrub/farmland profiles showed a bimodal shape depicting the four seasons observed in southern Ghana. The NDVI (Group A) made up of profiles 16, 17, 18 and EVI (Group A) also represented by the profiles 14, 15, 16, and 17. The maximum indices values were reached between the middle of April – to the end of July (*105 – 209 Julian days*) and from the middle of September – to the middle of November (*265 -329 Julian days*). (Appendix 4 tabulates these calendar days).

Group B: This unit consists of EVI and NDVI profiles representing bare/grassland cover type. The NDVI map is represented by a standalone profile, 12; and the EVI map by profiles 8, 9, 10. This unit also shows two peaks representing the two farming seasons, nonetheless, the relatively flatter nature of the profile identifies them with bare and grassland condition. This was confirmed by comparing the VI maps with the ASTER cover map. The higher NDVI values range between the start of October to the end of November; and also for the month June representing the minor and major wet seasons. And also, the dry season showing lower NDVI values spans between the beginning of January to mid-March and the month of August. In the case of the EVI, the higher values spanned between the middle of September to the start of November; and also, the month of June. The lower values showed up for July ending and the month of August, and also between the end of December to middle of February.

Group C: The NDVI profiles 2, 4, 5, 6, 9; and EVI profiles 2, 3, 4, 5, 6, 7 represent built ups. The relatively flatter graphs denote the general uniform condition of the area, even though effects from vegetation still existed. This is due to the close proximity between settlements and vegetation causing mixed pixels effect.

Group D: The graphs representing forest also shows bimodal shapes. NDVI profiles 8, 9, 10, 11, 13, 14, 15 and EVI profiles 11, 12, 13 showed resemblance to forests when compared to ASTER map. The December to March (22 -34) period on graph depicts the dry season. Also, by observation, the NDVI graph is relatively flat.

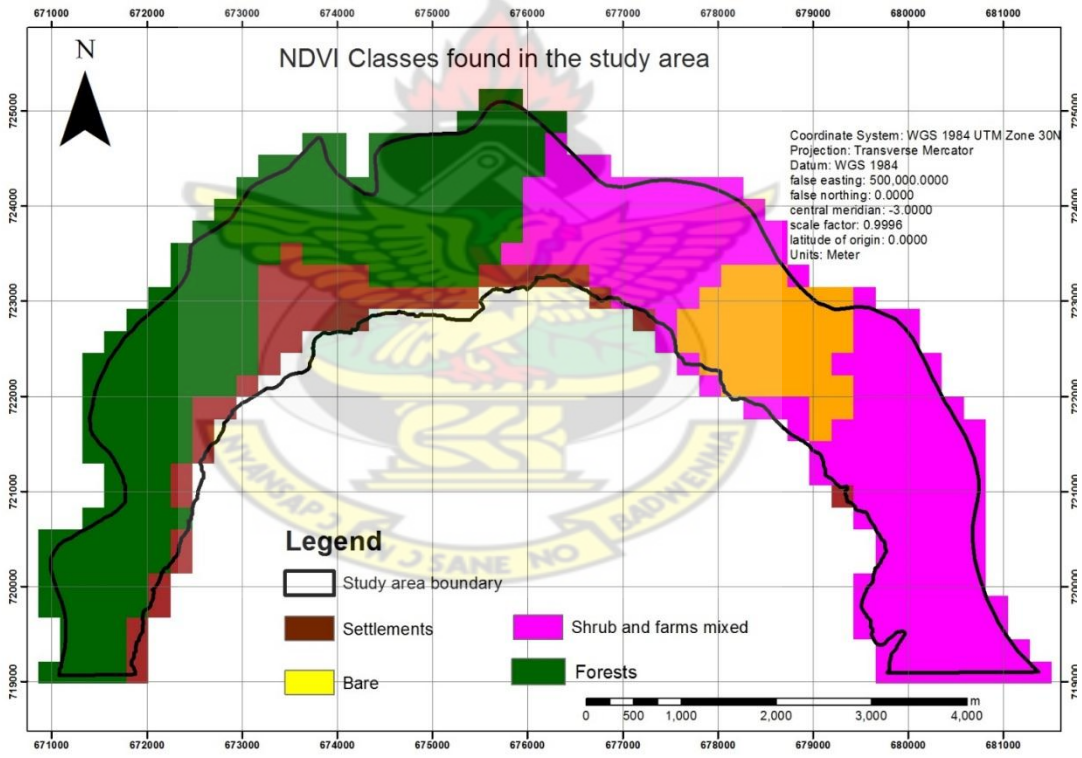

Figure 13: NDVI classes map produced from supervised classification based on mean NDVI profiles.

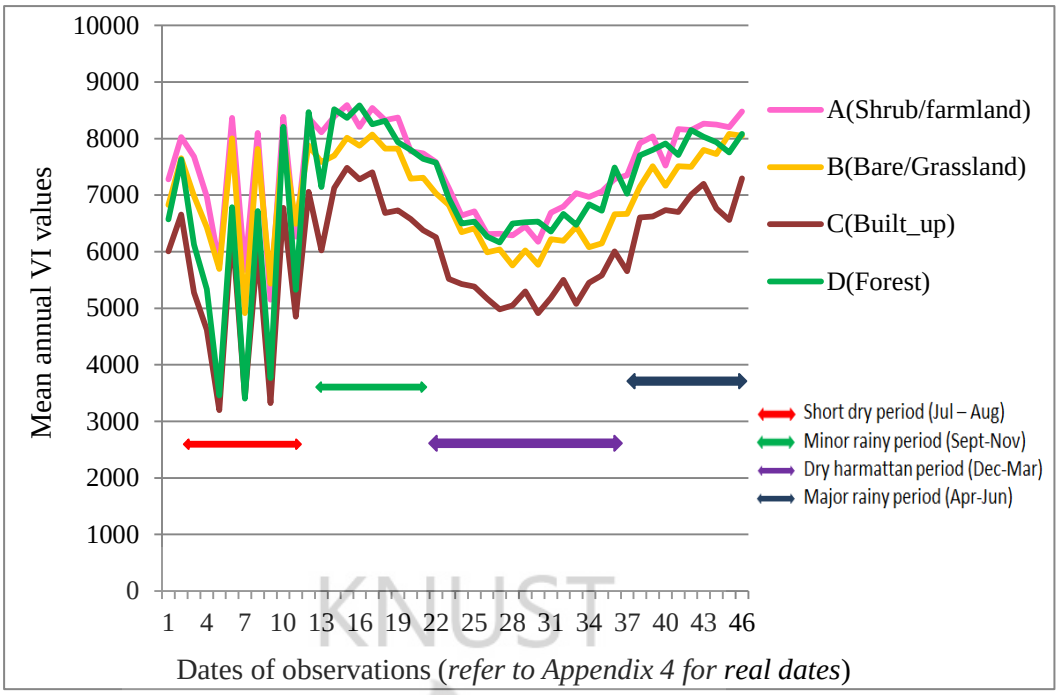

Figure 14: NDVI mean profile values representing 4 classes.

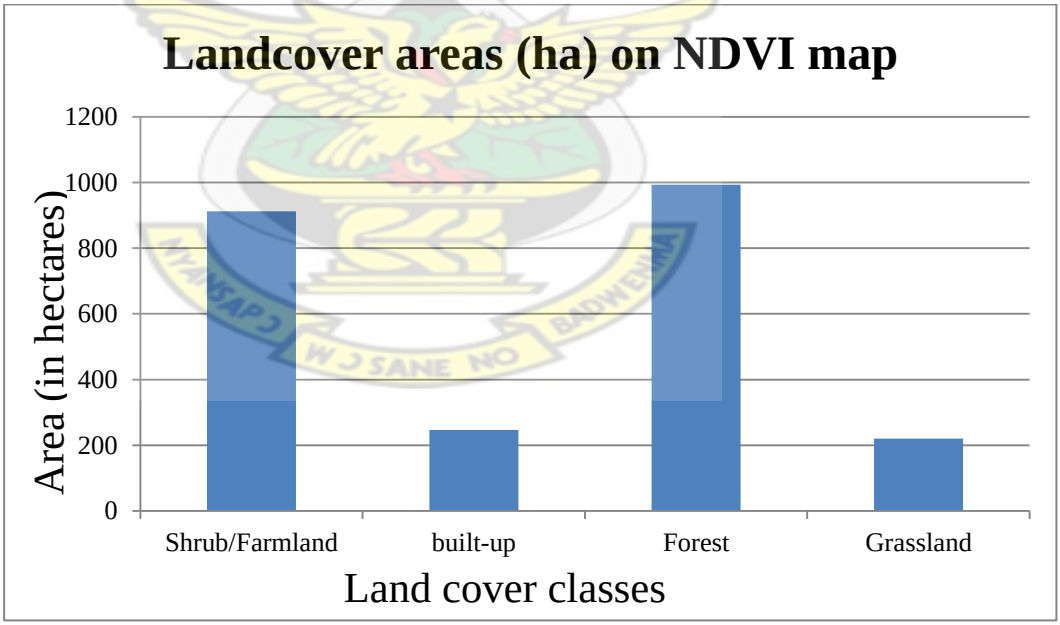

Figure 15: Area in hectares of the cover classes on NDVI map

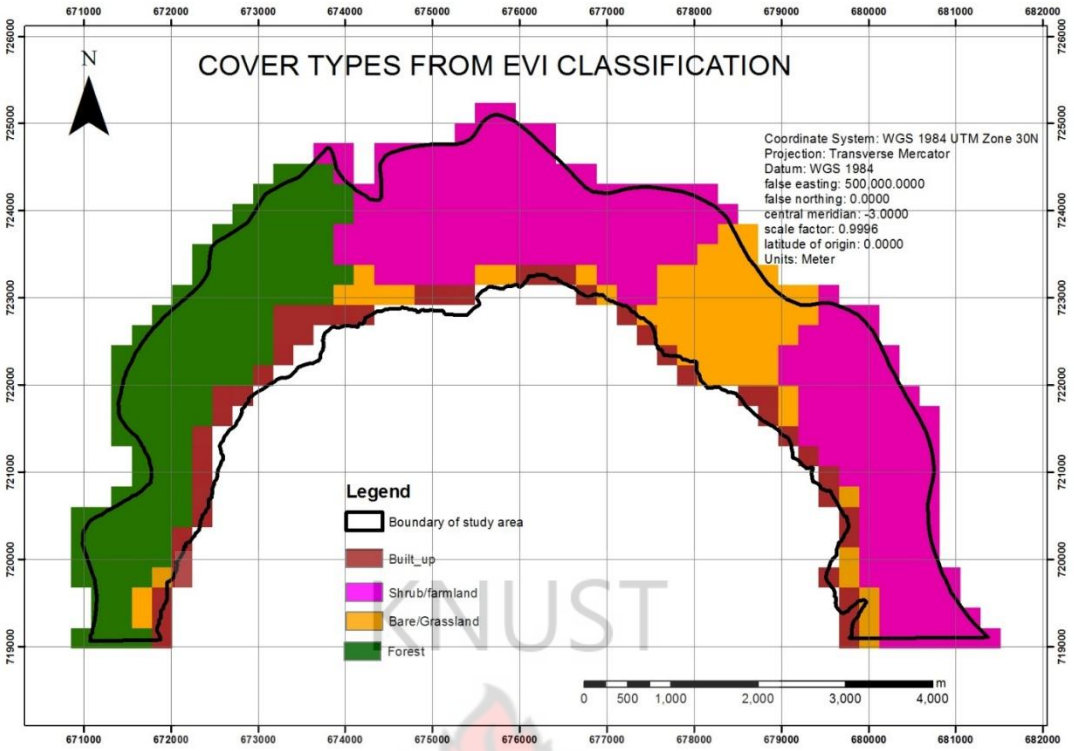

Figure 16: EVI classes map produced from supervised classification based on mean EVI profiles.

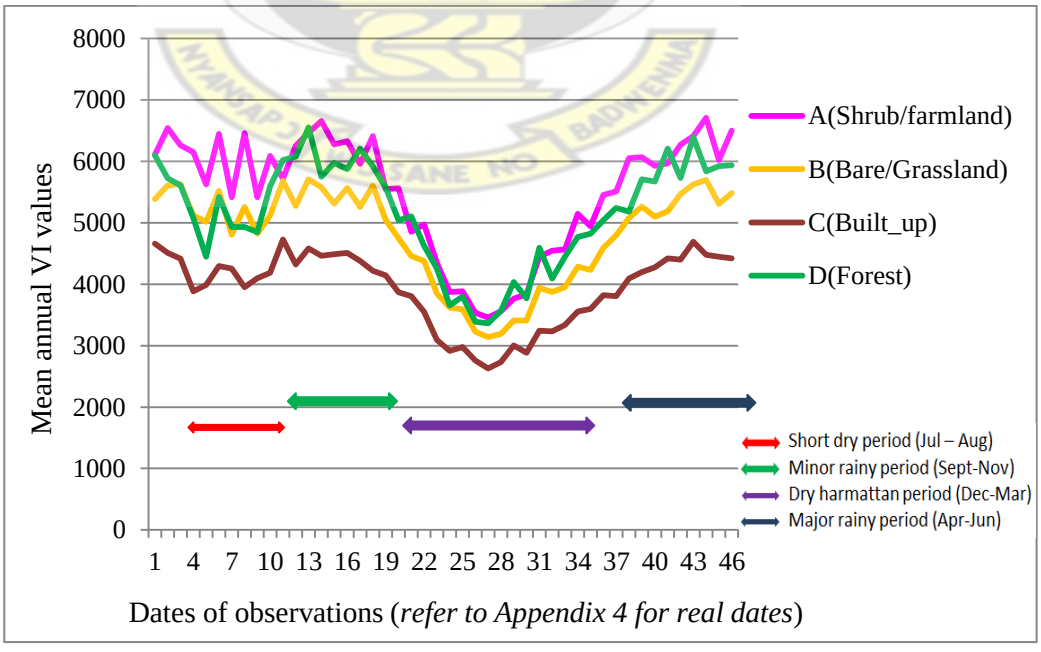

Figure 17: EVI mean annual profile values representing 4 classes.

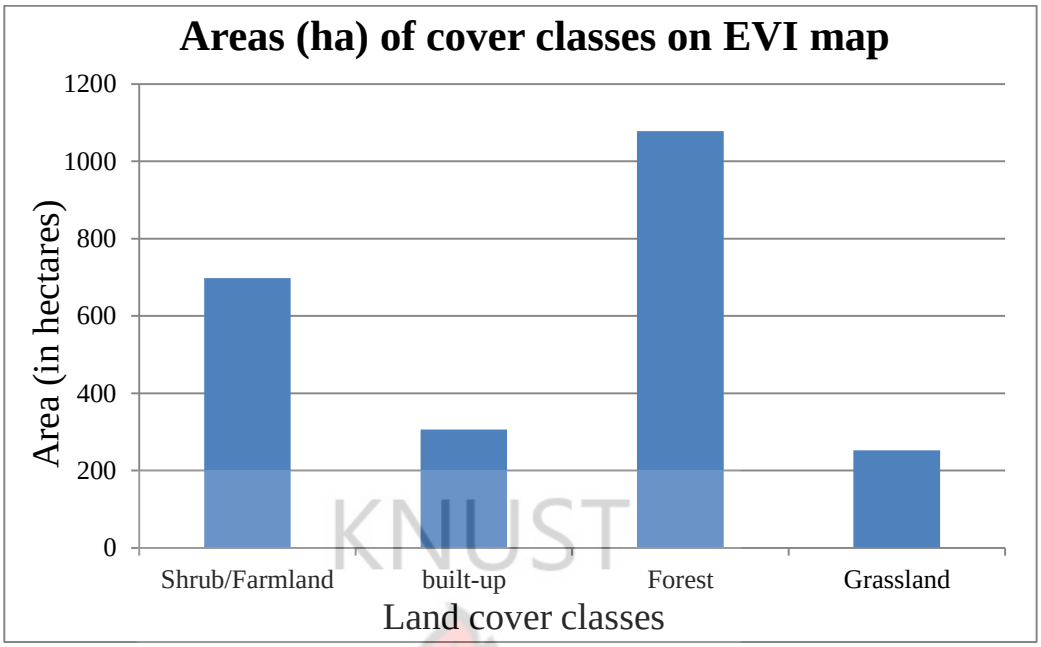

Figure 18: Area in hectares of cover classes on EVI map

3.2.3. Accuracy assessment of EVI and NDVI classification maps

The classified landcover map of ASTER provided the basis for the validation of the vegetation indices (VIs) classified maps. The producer's accuracy of the EVI are very high, forest cover recording the highest at 81.5% , followed by Shrub/farm and bare/built-up classes respectively at 77.5 and 72.9, respectively. The user's accuracy was 83.6% for bare /built-up, 78.2% for shrub/farmland and the lowest 75.8% for forest. The overall accuracy was 80.2% and overall kappa statistic is 0.71

Table 10: Classification error matrix of EVI cover map

Classification	Shrub/farm	Bare/Built-up	Forest	Total	Error of commission (%)
Shrub/farm	**86**	4	20	**110**	21.8
Bare/Built-up	3	**51**	7	**61**	16.4
Forest	22	15	**119**	**56**	66.1
Total	**111**	**69**	**146**	**326**	
Error of omission (%)	22.5	27.5	18.5		

Table 11: Classification accuracy assessment results for EVI cover map

Landcover class	Reference totals	Classified totals	Correct	Producer's Accuracy	User's Accuracy
Shrub/farm	111	110	86	77.48%	78.18%
Bare/Built-up	70	61	51	72.86%	83.61%
Forest	146	157	119	81.51%	75.80%

Overall Classification Accuracy = 80.22%

Overall Kappa Statistics = 0.7144

For the NDVI map, the highest producer accuracy was recorded for shrub/farm cover types with the value of 74.8%, this was followed by forest at 70.6% and bare/built-up at 55.7%. Forest has the highest user accuracy of 71%, followed by bare/built-up at 65% and lastly shrub/farm at 64.8%.

Table 12: Classification error matrix of NDVI cover map

	Shrub/farm	Bare/Built-up	Forest	Total	Error of commission (%)
Shrub/farm	**83**	17	28	**128**	35.2
Bare/Built-up	6	**39**	15	**60**	35
Forest	22	13	**103**	**138**	25.4
Total	**111**	**69**	**146**	**326**	
Error of omission (%)	25.2	43.5	29.5		

Table 13: Classification accuracy assessment results of NDVI cover map

Landcover class	Reference totals	Classified totals	Correct	Producers Accuracy	Users Accuracy
Shrub/farm	111	128	83	74.77%	64.84%
Bare/Built-up	70	60	39	55.71%	65.00%
Forest	146	145	103	70.55%	71.03%

Overall Classification Accuracy = 70.05%

Overall Kappa Statistics = 0.5677

3.2.4. Selecting the better vegetation index: NDVI verses EVI.

The study's main aim is to observe the performance of MODIS NDVI and EVI in classifying cover types to select one to be applied in USLE's *C* – factor's modeling. Accuracy assessment was used to select the better index for the next stage. The choice was based on the overall classification accuracies and kappa statistics of the two indices when assessed. For the EVI, 80% overall classification accuracy and 70% kappa statistic places it ahead of the NDVI which has values of 70% classification accuracy and 57% kappa statistic. The conclusion drawn, therefore, is that EVI is better in separating cover types between the two vegetation indices.

3.3. Estimating the USLE-*C* - factor map from best vegetation index

The EVI gave the best results in the separability analysis by visual inspection and statistical analysis; thus it was applied in modeling the *C*-factor. The exponential function method of *C*-factor modeling was used to convert the EVI's to models. First of all, four seasonal *C* – factor maps were developed for the periods spanning between April and June, July – August, September – November; and December – March. The *C*–map for the major rainy season which is the period spanning between April and June - which represents the major rainy season in Ghana - had *C* – values ranging from 0.0369 to maximum value of 0.598 (figure 24). The July to August dry period had 0.0318 – 0.553 range of *C*- values (figure 25). Also, the shorter minor season of September to November gave *C* – values of 0.017 to 0.541(figure 26). Lastly, the dry harmattan period of December to March showed values ranging from 0.154 to 0.666, (figure 27). An annual C – map shown in Figure 15 was produced by aggregating all the images for the 2010 year (shown in figure 20 and 21).

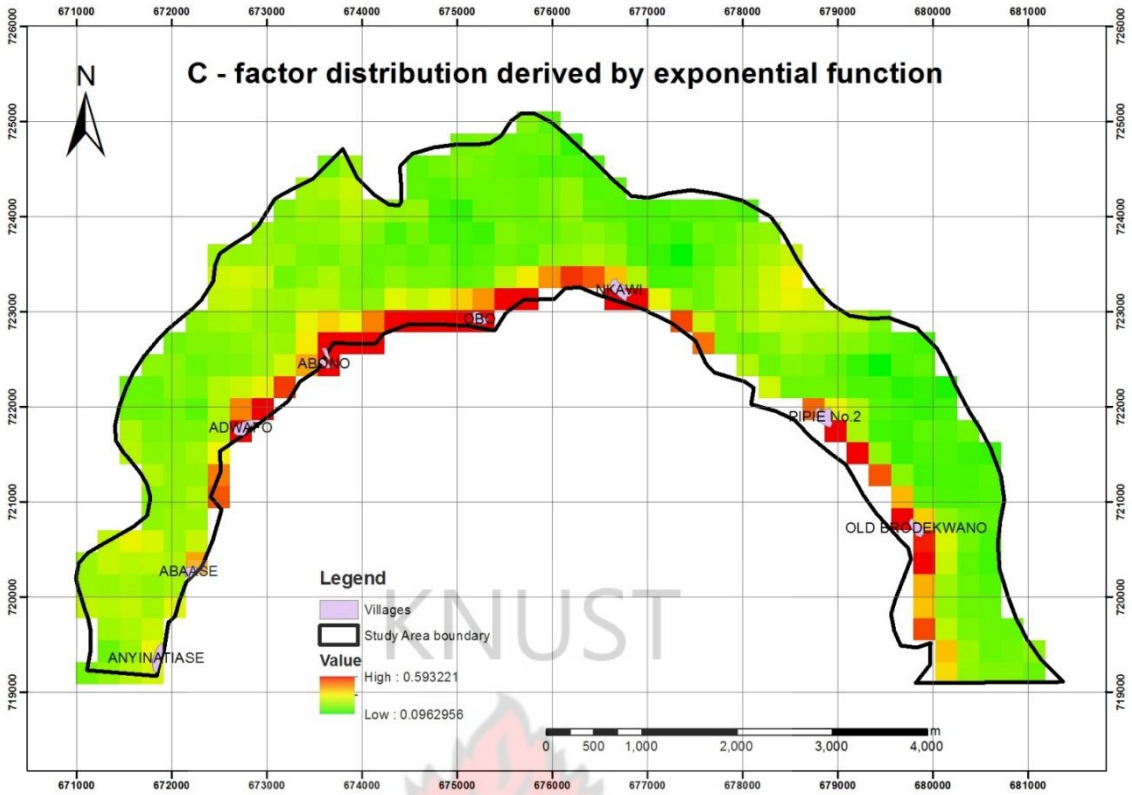

Figure 19: C - factor model developed from MODIS EVI

2.3.1. Validating *C*-factor map

The exponential function C – factor map was validated using the landcover C – factor map as the reference. The highest producer accuracy occurs for class range 0.0 – 0.1, followed by 0.1 – 0.2. The 0.5 – 0.6 has 0.0% and the rest of the classes have no value, since there were no classified total values for them. The users accuracy, 0.1 – 0.2 had the highest value, followed by 0.0 – 0.2. The 0.5 – 0.6 classes again had 0.0% and the rest of the classes, no value. The result shows an overall accuracy value of 76.7% and kappa statistic of 0.6. Base on the kappa coefficient, the 0.6 value means 60% of the classification agrees with the reference. The error and accuracy matrices are found in table 14 and table 15 below. Figure 19 shows the reclassified C – map.

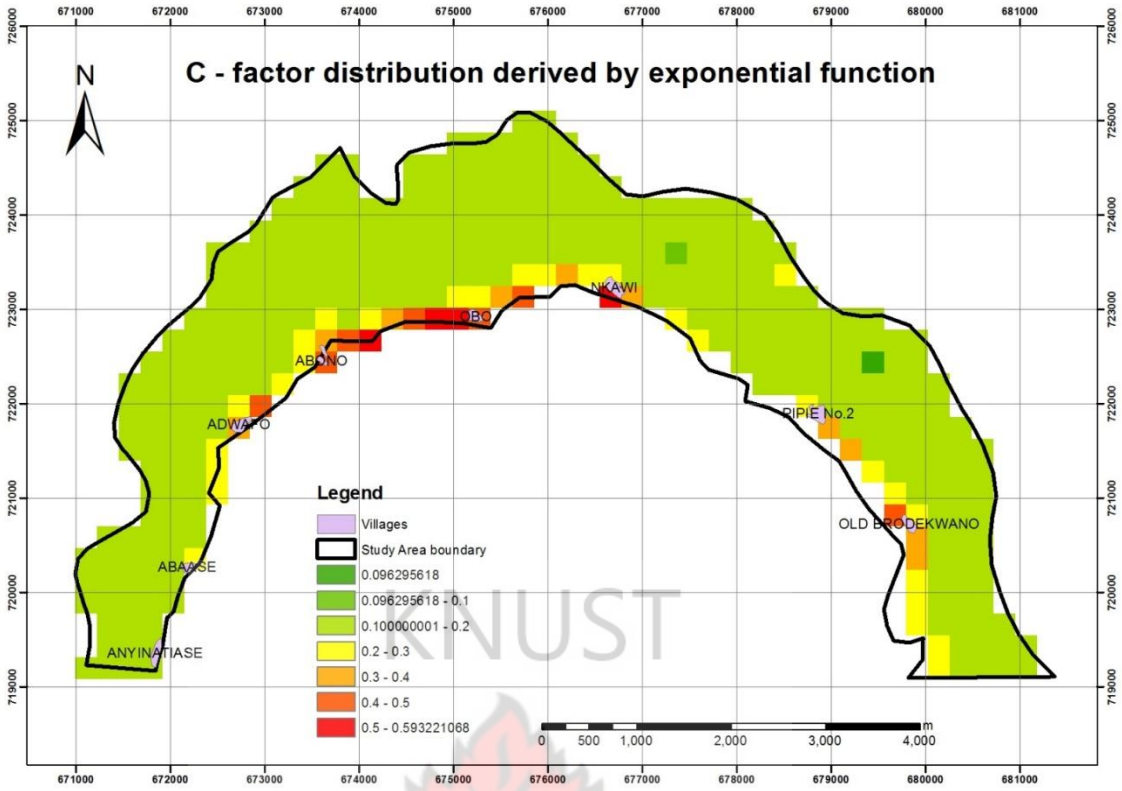

Figure 20: Reclassified C - factor map for the study area.

Table 14: Classification error report for C-factor model validation

C-factors	0.0 – 0.1	0.1 – 0.2	0.2 – 0.3	0.3 – 0.4	0.4 – 0.5	0.5 – 0.6	Total	Error of commission (%)
0.0 – 0.1	**171**	33	7	0	0	0	**211**	18.95
0.1 – 0.2	1	**109**	1	1	1	0	**113**	0.04
0.2 – 0.3	0	0	**0**	0	0	0	**0**	0
0.3 – 0.4	0	0	0	**0**	0	0	**0**	0
0.4 – 0.5	0	0	0	0	**0**	0	**0**	0
0.5 – 0.6	0	4	3	0	0	**0**	**7**	100
Total	**172**	**146**	**11**	**1**	**1**	**0**	**331**	
Error of omission (%)	0.006	25.5	100	100	100	0		

Table 15: Classification accuracy assessment report for C-factor model

C-factors	Reference totals	Classified totals	Number correct	Producers Accuracy	Users accuracy	Kappa
0.0 – 0.1	172	211		99.42%	81.04%	0.641
0.1 – 0.2	156	113		69.87%	96.46%	0.938
0.2 – 0.3	20	0	0	-	-	0.000
0.3 – 0.4	6	0	0	-	-	0.000
0.4 – 0.5	7	0	0	-	-	0.000
0.5 – 0.6	4	7	0	0.00%	0.00%	-0.011

Overall Classification Accuracy = 76.71%

Overall Kappa Statistics = 0.6087

3.3.2. Comparing *C*-factor maps to VI land cover map

A large area of the study site has *C* – value of 0.1 – 0.2. The *C*-factor distribution assessment for each of the cover types has shown that most of the cover types have *C*-factor values falling within the 0.1 – 0.2 *C*-factor class. It consists of forest cover type recording the highest, followed by shrub/farmland, bare/grassland and finally, built – up cover types. The built-up cover type dominates in the *C* – factor classes above 0.2. These are illustrated by figure 22 and 23, below.

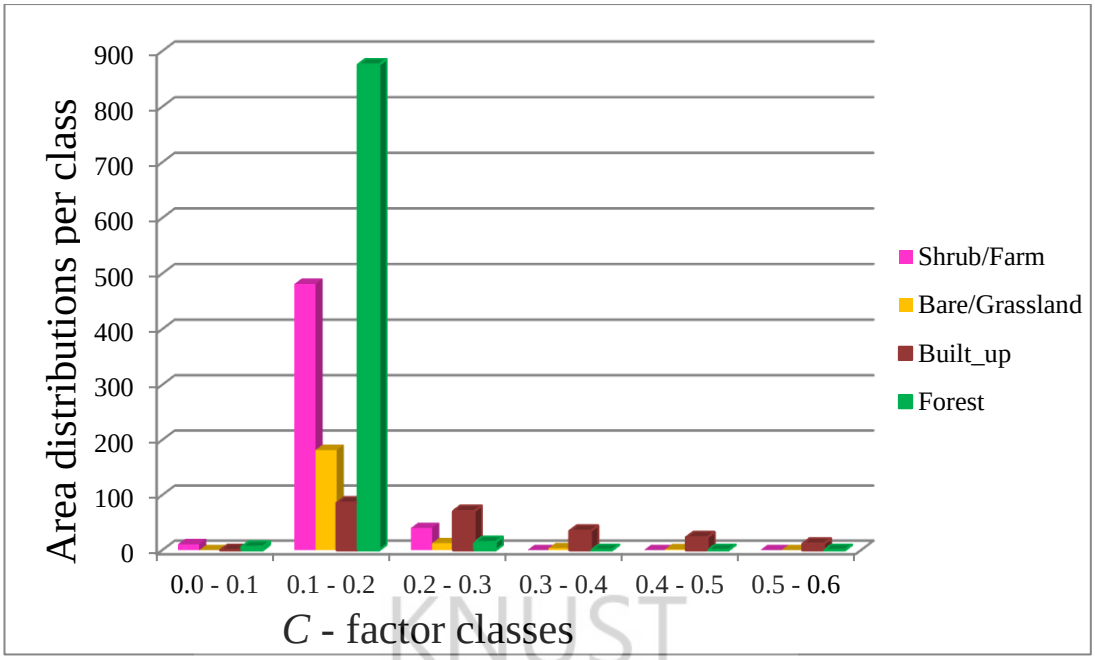

Figure 21: Area distribution of cover classes in each *C* - factor group.

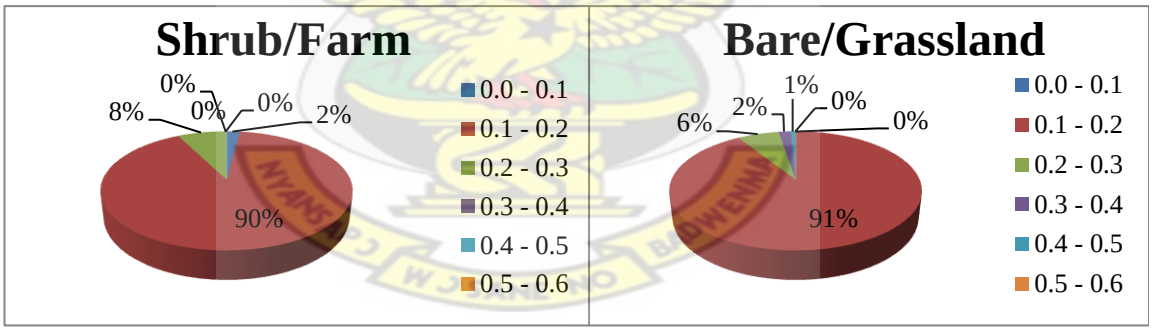

i. *C* – factor distribution for Shrub/farm cover type

ii. *C* – factor distribution for bare/grass cover type

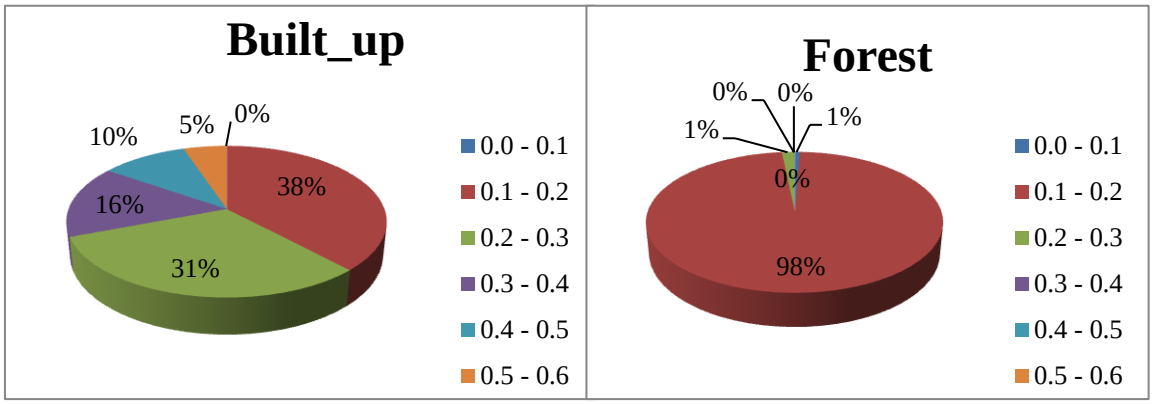

iii. *C* – factor distribution for Built - up landcover

iv. *C* – factor distribution for Forest landcover

Figure 22: C - factor values distribution within each of the EVI map classes.

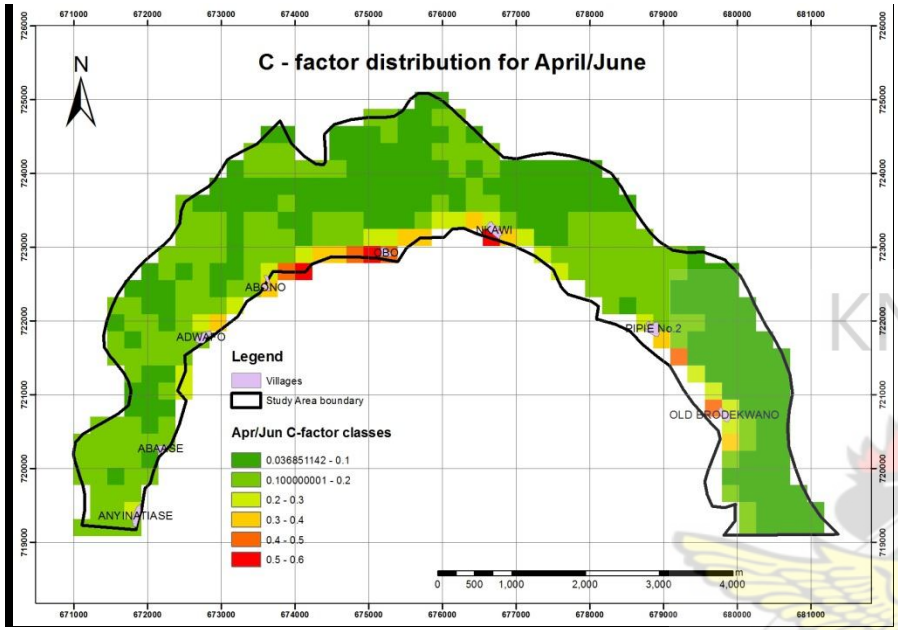

Figure 23: C - factor map for the major raining season

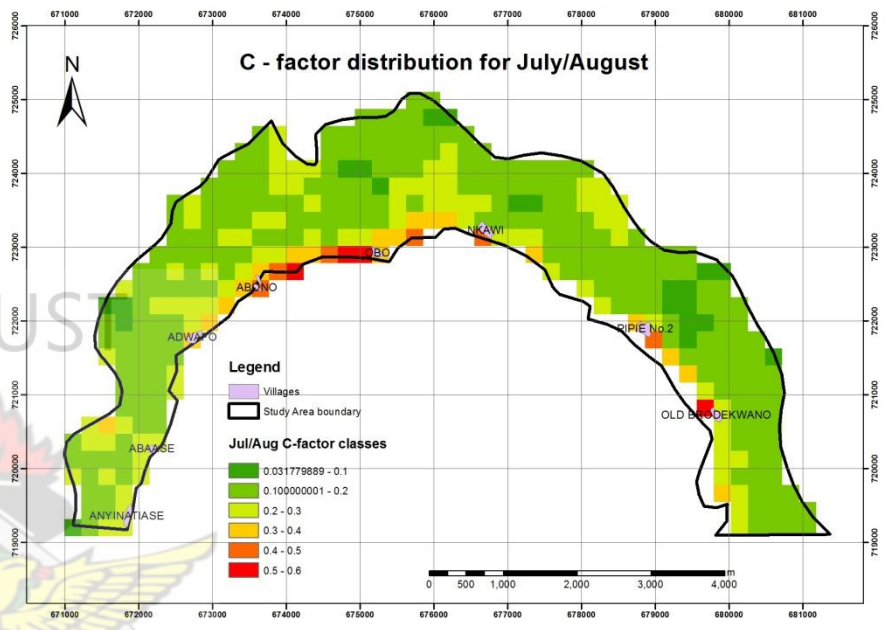

Figure 24: C - factor map for the July/August dry period

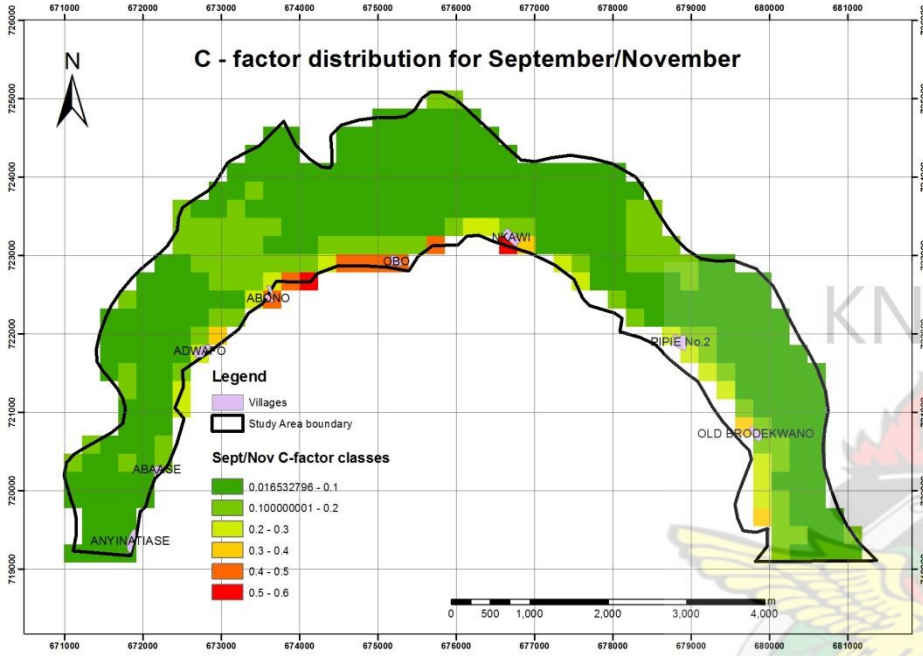

Figure 25: C - factor map for the minor raining season

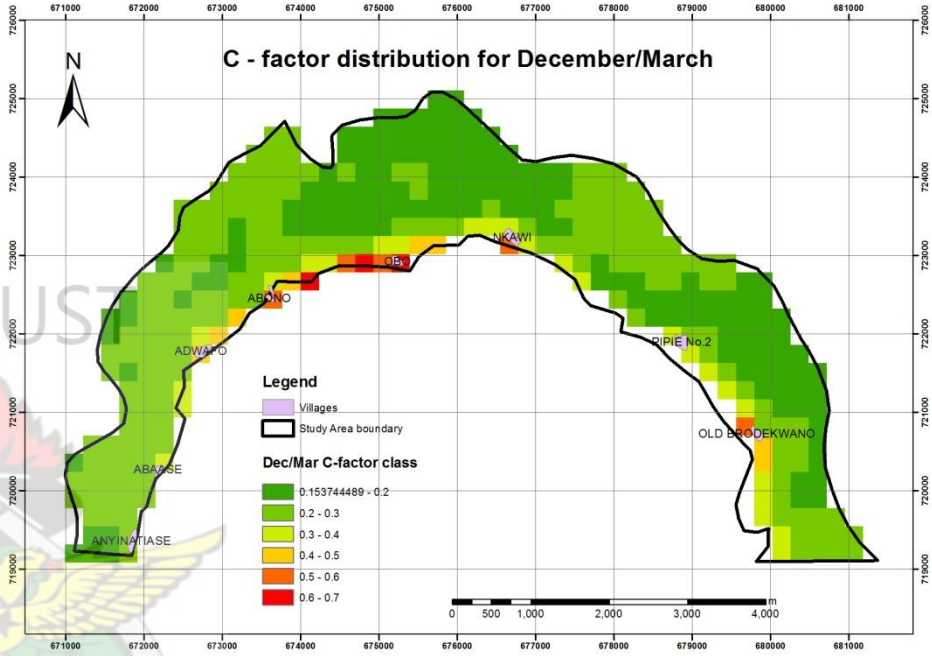

Figure 26: C - factor map for the harmattan dry period

4.0 DISCUSSION

The basic outputs of this research are the thematic landcover maps from ASTER 2010, Hypertemporal MODIS EVI and NDVI (2002 – 2010 images), C – factor maps and statistics. The following sections elaborate on these aspects of the output.

4.1. Accuracy assessment and land use/cover classification

The overall land use/cover classification accuracy of the ASTER image was 85% and kappa statistics 0.7924. These outputs show good conformity between the classification and the real land use/cover classes with few misclassified pixels occurring in some cover types. The accuracy level achieved is within 85 % and 90% classification accuracy standards established by Campbell (2002) and Lins & Klecker (1996).

Majority of the misclassifications that occurred are due to similar pixel values and mixed pixels. Among the four landcover types (forest, shrub, farmlands and bare/built-ups) discriminated from ASTER satellite image on the basis of spectral values and ground truth. It was difficult to separate bare from built-up therefore the two classes were merged. The similar pixel values can be attributed to the single time ASTER image captured in the dry season; specifically on the 4th of February, 2010; as well as the missing short-wave infrared band of ASTER. The shrub and farmland cover types also had few misclassified pixels based on their spectral properties. This difficulty can be explained to have resulted from the similarity of the canopy cover of both landcover classes. The agricultural practice is mostly mixed cropping, where percentage vegetation cover ranges from 60 to 100%, and that of the shrub, mostly above 90%. The vegetation cover in Bosumtwi basin is extremely heterogeneous, probably due to the landform and human activities. The highly variable vegetation

consists of farmlands, forest patches, shrubs, and farm fallows. This therefore explains the relatively low accuracy values observed for those classes. The farmland for instance, gave low producers' and users' accuracies of 53.9% and 50%; and a specific kappa value of 0.4.

4.2. ISODATA Clustering and supervised classification of Hypertemporal VI data

The output of the ISODATA clustering algorithm for both indices provided the clue for how many optimal classes; the vegetation index (VI) could be put into, through supervised classification. The optimal classes' numbers of 21 and 20 giving by the divergence statistic graphs, for NDVI, and EVI respectively, showed there are similarities between the performances of both indices. This also reflected on the classified maps, as both map outputs are quite similar, except the NDVI map giving more classes which were later found to belong to built-up cover type. Studies have proved that the NDVI is capable of mapping patchy areas compared to forested regions.

The supervised classification of the VI images using index profiles was however difficult with visual assessment as was done in previous studies (de Bie, *et al.*, 2008) due to the similarity existing between the

mean VI profile values representing the different cover types. This non - distinguishable nature of the VI values is as a result of the mixed signals received from the ground for each pixel. This therefore lead to spectral overlap of classes (mixed pixels). This observed complicating issue was as a result of the disparity between the image pixel size and the average patch size of the basin. Thus, the heterogeneous

nature of the study area and the patchy size nature of the cover types explain why some of the cover types could not be clearly discriminated by the 250m resolution multi-temporal MODIS images. The dendrogram statistical tool of SPSS therefore helped group the mean VI profiles into four categories, which was subsequently applied in grouping the corresponding classes on the VI maps as well.

4.3. Legends matching with cover types

The four classes shown on the VI maps depict the major classes when compared to the landcover map developed from ASTER. It was observed that, the multi-temporal VI maps could not separate very well different cover classes. This can be attributed to the similar nature of these cover types and the pixel resolution of the MODIS image. For instance, the mixed farms and shrubs could not be well discriminated on the MODIS VI maps, which however was separated with the high resolution single date ASTER map. That explains why the farm (in exception of cocoa farms) and shrub classes were merged as one unit. Nonetheless, for contiguous fields; the vice versa occurred, where the MODIS multitemporal image used was an advantage. The VI profiles were useful in delineating settlement from bare/grass cover types whereas the single date ASTER could not. Mitsuzuka and Ohira, (*website*), resolved that there is problem associated with mapping forest by satellite imagery captured in the dry season due to defoliation, nonetheless data captured in the rainy season is also concealed by cloud. Therefore, time-series VI composites application seems to be the only way out.

The overall pattern of the landcover profiles appear to be in line with the climatic patterns, which is due to the Inter Tropical Convergence Zone (ITCZ) in Africa (Landsberg, 1972 as cited in Jönsson and Eklundh, 2004). All the classes' profiles showed bimodal pattern over the years illustrating the two wet seasons and dry seasons observed in southern Ghana. The two dominant cover types: forest and

shrubs/farmlands showed highest VI values. All the cover types showed high values during the two wet seasons and low values during the dry periods. It is not normal for non-forest cover types to exhibit seasonal variation pattern as forest cover types; nevertheless, the impact of the mixed pixels (mixels) explains these bimodal observations made for built – up cover types. These results are partly confirmed by the observations made by Mitsuzuka and Ohira, (*website*) in their study area of Cambodia, that MODIS time-series index is suitable for mapping forests from non-forest; however, it cannot be used to classify other covers. The best outputs that can be observed are mixed pixels, and this was observed in the built-up and bare cover types. The ability of this study to delineate bare/grass cover types was however an improvement on the results of Mitsuzuka and Ohira, (*website*). The outcome is that the VI seasonal variation shape becomes changeable based on the mixture part of those mixed pixels (*mixels*) and ultimately, not enabling the classification to be obtained (Mitsuzuka and Ohira, *website*). The built-up and grass profile groups are however distinguished by the relatively flatter shape when compared to other cover types.

4.4. Accuracy assessment of EVI and NDVI classification maps

The overall accuracy of the EVI classification map is 80.22; this falls within the overall accuracy (80 – 85%) regarded as good (Treitz and Rogan, 2004). The results of the accuracy assessment of the ASTER cover map with a value of 84.5%; is alright (Lins & Klecker, 1996); and thus was used as the reference for assessing the accuracy of the moderate resolution VI MODIS images. Distinction among the cover types in the basin was difficult to make, hence, dominating cover types were assigned to the observed classes. In spite of these difficulties, some classes are recognized with high accuracy. For instance, forest gave the highest producers' accuracy of 81.5% and also, shrub/farm with 77.5%. The users' accuracies for the three classes are also quite

substantial. The 70% total kappa statistic of the EVI map is also significant. The total classification accuracy of the NDVI 70% and the total kappa statistic is 57%. Both the producers' and users' accuracy for bare/built-up is low.

4.5. Selecting the better vegetation index: NDVI verses EVI.

The EVI was selected as the best separating vegetation index. The study's main aim is to observe the performance of MODIS NDVI and EVI in classifying cover types to select one to be applied in USLE's *C* –factor's modeling. Accuracy assessment was used to select the better index for the next stage. The choice was based on the overall classification accuracies and kappa statistics of the two indices when assessed. The 80% overall classification accuracy and 0.7 kappa statistics of the EVI places it ahead of the NDVI with accuracy and kappa values of 70% and 0.57.

4.6. The spatial C-factor maps modeling and validation

The *C* – values vary throughout the year due to changes in landcover type, hence when modelling *C* – factor map; consideration must be given to the temporal variation (Gitas, *et al.*, 2009). *C*–factor maps produced to represent the four different seasons in Southern Ghana also showed this trend. The major (May – June) rainy season *C* – values which ranges from 0.0369 to 0.598 (figure 22), and that of July to August (0.0318 – 0.553) shows similar rages. This can be attributed to the fact that the conditions during those periods are usually comparable for the study area. The distinction exists between the first two periods and the shorter minor season of September to November and the dry harmattan period of December to March. The range of *C* – values of 0.017 to 0.541for the former is comparatively lower than the rest. While the dry harmattan season showed values relatively higher (0.154 to 0.666) than the other groups. The dry season is the period that plant leaves senescence and

thereby resulting in higher *C* – factor values which will ultimately result in higher erosion risk with the values produced by the other factors.

The mean *C*-factor value averages all these periods and can used as the annual cover and management factor for USLE erosion modelling after validation of the results. The validated results for the annual *C*-factor map was significant but can be improved with maps from higher resolution images and more specific *C*- factor values.

5.0. LIMITATIONS, CONCLUSIONS AND RECOMMENDATIONs

5.1. Limitations

The mapping of the study area was problematic because of the resolution of the existing satellite image. Improved results can be obtained with better geometric and spectral resolution imagery. Mati, (1999) as cited in Mati and Veihe (2001) in a comparative studies of Ghana and Kenya with high resolution Landsat image, made the observation that it is difficult to delineate spatial variation in crop cover for fragmented farm plots in Ghana compared to Kenya.

The studies made use of the traditional approach for *C*- mapping to validate the output model with literature assigned values. But literature *C* – values used for the validation, can also be bias. *C* –factor values for inter-cropping and agroforestry practices in Ghana and West Africa as a whole are non-existent (Mati and Veihe, 2001). Therefore, the validation results used in this study might be improved with improved and more specific *C* – values.

5.2. Conclusions

Following research question 1:

Can the distribution of landcover types in the basin be mapped with high accuracy using?

i. ASTER image and

ii. Hypertemporal MODIS derived vegetation indices?

The results of the landcover mapping from ASTER image and Hypertemporal MODIS VIs showed that:

- The landcover map from ASTER image produced 85% overall accuracy and kappa statistics of 0.7924
- The spectral similarities between built-up and bare/grassland cover types; and also, shrubs and farmlands cover types were very similar.
- The divergence statistics plots showed that the NDVI and EVI can be optimally classified into 21 and 20 distinctive cover units, respectively.
- The 21 NDVI and 20 EVI cover units were put into four classes each based on combinations of visual and statistical analysis. These classes are shrub and farmland, built up, bare and grassland area, and forest classes.

This was due to the facts that it was a single time image and also the area being highly heterogeneous. However, the multispectral vegetation indices (VIs) maps slightly differ, the NDVI and EVI maps both showed distinctively the built-up and bare/grassland cover types.

Following research question 2:

Which index can be better applied to estimate *C* – factor for the Bosumtwi basin?

- There are similarities between the outputs of both indices, especially the divergence statistics. But the total accuracy assessment and kappa statistics values placed the EVI ahead of the NDVI. The overall accuracy assessment value for EVI is 80% and NDVI is 70%; the kappa statistics are 0.71 and 0.61 for EVI and NDVI, respectively.

The EVI was therefore chosen for the *C* – factor modeling.

Following research question 3:

How related are the predicted *C*-factor values to literature cited values?

- The Exponential function approach of *C* – factor estimation was applied to model *C*- factor for the whole basin for the year.
- A validation map was generated using the EVI classified map with assigned *C*-factor values derived from literature.
- An accuracy assessment of the *C*- factor map with landcover *C*- factor resulted as reference gave a value of 77% total accuracy and 0.61 kappa statistics value.

The traditional method of *C*- factor modeling is always less reliable, especially in areas of data scarcity.

5.3. Recommendations

The mixed class units observed in the MODIS indices classification maps could be solved using any of the sub-pixel analysis tools for instance the Sequential Maximum Angle Convex Cone (SMACC) endmember model (Research Systems Inc., 2005) and the Spectral Angle Mapper (SAM) algorithm. The SAM can separate two different classes by computing the angle between the spectra, by using the phenology spectra along with the image stack (Research Systems Inc., 2005, Kruse et al., 1993). Also, the SMACC tool, purposely designed to find end members from calibrated hyperspectral data, could aid in separating settlements areas from other cover classes on stacked MODIS temporal image of a heterogeneous study area. The two algorithms together can be used to give two detail maps, each for NDVI and EVI, to be compared.

Other uncommon indices can be compared, especially, indices using bands outside the red and near infrared bands. Gong *et al.*, (2003) established that bands with longer wavelengths than near infrared were able to correlate better with certain plant chemicals and consequently, can be applied in determining vegetation metrics like fAPAR, vegetation cover, leaf area index (LAI), among others.

The output maps from the hyperspectral analysis could be correlated to biophysical data like rainfall, temperature and many others, to better understand the trend of the profiles.

Additionally, field measurements to relate *C*-factor to the remotely sensed data can also be explored.

A direct derivation of *C*-factor values from vegetation indices without field confirmation can be erroneous and does not reflect realty (Suriyaprasit & Shrestha, 2008). It will be necessary to derive *C*-factor values from vegetation cover, plant residue after crop harvest and soil surface cover; etc. according to the approach explained for RUSLE (Renard *et al*, 1997), but the time allowed for this research could not permit. That explained why existing literature *C*-factor values were assigned to the classes delineated on the ASTER classification map and used to validate the *C*-factor model.

6.0. REFERENCES

Ali, A. (2009). "Comparison of Strengths and Weaknesses of NDVI and Landscape-Ecological Mapping Techniques for Developing an Integrated Land Use Mapping Approach". *M. Sc. thesis*. University of Twente, Enschede, The Netherlands.

Amiri, F., and T. Tabatabaie. (2009). EPM Approach for Erosion Modeling by Using RS and GIS, ASCE.

Beck, P.S.A., C. Atzberger, K.A. Hogda, B. Johansen and A.K. Skidmore, (2006) "Improved monitoring of vegetation dynamics at very high latitudes: A new method using MODIS NDVI", Remote Sensing of Environment 100 (3), pp.321-334.

Beltran-Abuanza, J. (2009). Method development to process hyper-temporal remote sensing (RS) images for change mapping. *ITC M. Sc. thesis*. University of Twente, Enschede, The Netherlands.

Bhattarai R, Dutta D (2007) Estimation of soil erosion and sediment yield using GIS at catchment scale. Water ResourManag 21: 1635–1647

Boamah D. and Koeberl C. 2006. Petrographic studies of "fallout" suevite from outside the Bosumtwi impact crater, Ghana Meteoritics & Planetary Science 41:1761–1774.

Colditz, R. R., C. Conrad, T. Wehrmann, M. Schmidt, & S. Dech. (2006). Generation and Assessment of MODIS Time Series using Quality Information. Geoscience and Remote Sensing Symposium, 2006. IGARSS 2006. IEEE International Conference on.

Congalton, R. G. (1991). "A review of assessing the accuracy of classifications of remotely sensed data." Remote Sensing of Environment **37**(1): 35-46.

Crippen, R.E., (1990) "Calculating the vegetation index faster" Remote Sensing of Environment. Elsevier, 341, (71-73)0034-4257.

de Bie, C.A.J.M., Khan, M.R., Toxopeus, A.G., Venus, V. and Skidmore, A.K., 2008. "Hypertemporal image analysis for crop mapping and change detection". In: ISPRS 2008 : Proceedings of the XXI congress : Silk road for information from imagery : the International Society for Photogrammetry and Remote Sensing, 3-11 July, Beijing, China. Comm. VII, WG VII/5. Beijing : ISPRS, 2008. pp. 803-812.

De Jong, S. M. (1994). "Application of Reflective Remote Sensing for Land Degradation Studies in a Mediterranean Environment" (Utrecht: Netherlands Geographical Studies, University of Utrecht)

De Jong, S.M., Paracchini, M.L., Bertolo, F., Folving, S., Megier, J., and De Roo, A.P.J. (1999)."Regional assessment of soil erosion using the distributed model SEMMED and remotely sensed data". Catena 37 (3–4), 291–308.

Demirci, A. and A. Karaburun (2011) "Estimation of soil erosion using RUSLE in a GIS framework: a case study in the Buyukcekmece Lake watershed, northwest Turkey." Environmental Earth Sciences: 1-11.

Deng, X., J. Huang, S. Rozelle, and E. Uchida. (2008). "Growth, population and industrialization, and urban land expansion of China." Journal of Urban Economics **63**(1): 96-115.

Epiphanio, J. C. N. and A. R. Huete (1995). "Dependence of NDVI and SAVI on sun/sensor geometry and its effect on fAPAR relationships in alfalfa." Remote Sensing of Environment 51(3): 351-360.

Erencin, Z. (2000). "C-Factor Mapping Using Remote Sensing and GIS. A case Study of Lom Sak/Lom Kao, Thailand." International Institute for Aerospace Survey and Earth Sciences (ITC).

Folly, A., Bronsveld, M., and Clavaux.M., (1996).“A knowledge-based approach for C-factor mapping in Spain using Landsat TM and GIS”. International Journal of Remote Sensing, 17 (12), 2401-2415.

Gitas, I. Z., K. Douros, C. Minakou, G.N. Silleos and C.G. Karydas.. (2009). "Multi-temporal soil erosion risk assessment in N. Chalkidiki using a modified USLE raster model." EARSeL eProceedings **8**(1):40-52.

Gitelson, A. A. (2004). “Wide Dynamic Range Vegetation Index for Remote Quantification of Biophysical Characteristics of Vegetation”.Journal of plant physiology. 161. 165 – 173.

Gong, P., Pu, R., Biging, G. S. and Larrieu, M. R. (2003). "Estimation of forest leaf area index using vegetation indices derived from Hyperion hyperspectral data." Geoscience and Remote Sensing, IEEE Transactions on **41**(6): 1355-1362.

Haan, C.T., Barfield, B.J. and Hayes J.C. (1994).*Design Hydrology and Sedimentology for Small Catchments*. Academic Press, Inc, California.

Khosrowpanah, S., Heitz, L., Wen, Y., and Park, M. (2007). “Developing a GIS-based Soil Erosion Potential Model of the Ugum Watershed.” Technical Report

Holben, B. N., C. J. Tucker, Fan, C.J. (1980). "Spectral assessment of soybean leaf area and leaf biomass." Photogrammetric Engineering and Remote Sensing **46**: 651-656.

Huete, A. R. H. Q. Liu, K., batchily, W. van Leeuwen (1997). A Comparison of Vegetation Indicex over a Global Set of TM images for EOS-MODIS, Remote Sensing of Environment, vol. 59, pp. 440 – 451.

Huete, C. Justice and W.V. Leeuwen,(1999) "MODIS vegetation index (MOD13): algorithm theoretical basis document".

Huete, A., K. Didan, T, Miura, E.P Rodriguez, X. Gao, and L.G Ferreira (2002). "Overview of the radiometric and biophysical performance of the MODIS vegetation indices." Remote Sensing of Environment **83**(1-2): 195-213.

Jackson, R. D., Slater, P. N., and Pinter, P. J. (1983). "Discrimination of growth and water stress in wheat by various vegetation indices through clear and turbid atmospheres." Remote Sensing of Environment **13**(3): 187-208.

Jensen, J. R. (2005). "Introductory Digital Image Processing: A Remote Sensing Perspective" Pearson Prentice Hall, New Jersey.

Jönsson, P. and L. Eklundh (2004). "TIMESAT--a program for analyzing time-series of satellite sensor data." Computers & Geosciences **30**(8): 833-845.

Karaburun, A. (2010). "Estimation of C factor for soil erosion modeling using NDVI in Buyukcekmece watershed." Ozean Journal of Applied Sciences**3**(1): 77-85.

Knight, J. F., R. S. Lunetta, J. Ediriwickrema, and S. Khorram. (2006). "Regional scale land cover characterization using MODIS-NDVI 250 m multi-temporal imagery: a phenology-based approach." GIScience & Remote Sensing **43**(1): 1-23.

Koeberl, C. and Reimold, R. U. (2005). "Bosumtwi Impact Crater: an updated and revised Geological Map, with explanations". Geologische Bundesanstalt.

Lal R (2001)."Soil degradation by erosion". Land Degrad Dev12:519–539

Lillesand, T. M., Kiefer, R. W., and Chipman, J. W. (2004). "Remote Sensing and ImageInterpretation" 5th ed. New York: John Wiley & Sons, Inc.

Lin, C. Y., Lin, W. T., and Chou, W.C. (2002). "Soil erosion prediction and sediment yield estimation: theTaiwan experience." Soil and Tillage Research**68**(2): 143-152.

Lu, D., G. Li, G. S. Valladares, and M. Batistella. (2004). "Mapping soil erosion risk in Rondonia, Brazilian Amazonia: Using RUSLE, remote sensing and GIS." Land Degradation & Development **15**(5): 499-512.

Mati, B. and A. Veihe (2001). "Application of the USLE in a savannah environment: comparative experiences from east and west Africa." Singapore Journal of Tropical Geography **22**(2): 138-155.

Millward, A. A. and J. E. Mersey (1999). "Adapting the RUSLE to model soil erosion potential in a mountainous tropical watershed." Catena **38**(2): 109-129.

Mitsuzuka, N., and Ohira, W. (*website*). "Advantage of MODIS time series NDVI data for forest situation analysis in case of Cambodia". *Japan Wildlife research center*. Tokyo, Japan. Accessed date: 20 – 04 – 2012. Website http://www.a-a-r-s.org/acrs/proceeding/ACRS2008/Papers/PS%202.15.pdf

Morgan, R. P. C. (2005). Soil erosion and conservation, Wiley-Blackwell.

Mróz, M., & A., Sobieraj (2004). "Comparison of Several Vegetation Indices Calculated on The Basis of A Seasonal SPOT XS Time Series, and their Suitability for Land Cover and Agricultural Crop Identification"Department of Photogrammetry and Remote Sensing

University of Warmia and Mazury, Olsztyn.

Mulianga, B. A. (2009). Modelling pastoral mobility to accommodate pastoral land use in land administration, a case study of the Isiolo Area, Kenya. *M. Sc. thesis.* University of Twente, Enschede, The Netherlands.

Ndirima, Z. (2007). Mapping and monitoring wetland vegetation used by wattled cranes using remote sensing : case of Kafue flats, Zambia. Enschede, *M. Sc. thesis* ITC**:** 69.

Neteler, M. (2005). "Time series processing of MODIS satellite data for landscape epidemiological applications." Int J Geoinf **1**: 133-138.

Ofosu, P. E, (2006). "Lake Bosumtwi, the pride of Ashanti". *Deszyn Origin Publishers.*

O'stir, K. and Halounova, H. (2005). Using of TM data and VHR data for reclamed areas monitoring using vegetation indices. The International Archives of the Photogrammetry, Remote Sensing and Spatial Information Sciences 34, Part XXX

Payero, J., C. Neale, J. L. Wright. (2004). "Comparison of eleven vegetation indices for estimating plant height of alfalfa and grass." Applied Engineering in Agriculture **20**: 385-393.

Prakash, S., Wieringa, P., Ros, B., Poels, E., Boateng, F. S., Gyampoh, B. A. & Asiseh, F. (2005): Potential of ecotourism development in the Lake Bosumtwi Basin: A case study of Ankaase in the Amansie East District, Ghana:-SEFUT Working Paper No. 15. Working Group Socio-Economics of Forest use in the Tropics and subtropics. University of Freiburg, Germany, 52 pp.

Purevdorj, T., R. Tateishi,T Ishiyama and Y. Honda. (1998). "Relationships between percent vegetation cover and vegetation indices." International Journal of Remote Sensing **19**(18): 3519-3535.

Rejman, J., Turski, R., and Paluszek, J. (1998). "Spatial and temporal variability in erodibility of loess soil." *Soil Tillage Res.* 46, 61-68.

Renard, K. G., Foster, G. R., Weesies, G. A., McCool, D. K., and Yoder, D. C. (1997). "Predicting soil erosion by water. A guide to conservation planning with the revised universal soil loss equation (RUSLE)."

Reusing, M., T. Schneider, and U. Ammer. (2000). "Modelling soil loss rates in the Ethiopian Highlands by integration of high resolution MOMS-02/D2-stereo-data in a GIS." International Journal of Remote Sensing **21**(9): 1885-1896.

Rouse, J.W., R.H. Haas, J.A. Schell, and D.W. Deering, (1973). *Monitoring Vegetation Systems in the Great Plains with ERTS*. Third ERTS Symposium, NASA SP-351 I: 309-317.

Rouse, J. W., Haas, R. H., Schell, J. A., Deering, D. W., & Harlan, J. C. (1974). "Monitoring the vernal advancement of retrogradation of natural vegetation" (p. 371). Greenbelt, MD: NASA/GSFC (Type III, Final report).

Scarrott, R. G. (2009). "Extracting gradient boundaries using hyper-temporal image analysis: progress towards a tool for gradient analysts". *M. Sc. thesis*. University of Twente, Enschede, The Netherlands.

Serban C., (Gherghina), Maftei, C., Filip, C. (2011) Assessment of Multi-spectral Vegetation Indices using Remote Sensing and Grid Computing. *INTERNATIONAL JOURNAL OF COMPUTERS:* 5(4).

Suriyaprasita, M. and D. Shresthab (2008). "Deriving Land Use and Canopy Cover Factor from Remote Sensing and Field Data in Inaccessible Mountainous Terrain for Use in Soil Erosion Modelling." The International Archives of the Photogrammetry, Remote Sensing and Spatial Information Sciences **37**: 1747-1750.

Townshend, J R. G. and C. O. Justice (2002). "Towards operational monitoring of terrestrial systems by moderate-resolution remote sensing." Remote Sensing of Environment **83**(1-2): 351-359.

Treitz, P.M., and J. Rogan, 2004. Remote Sensing for Mapping and Monitoring Land-Cover and Land-Use Change – An Introduction, In Remote Sensing for Mapping Land Cover and Land Use Change, Ed., P.M. Treitz, Progress in Planning 61(3): 269-279.

Tucker, C.J., (1979). "Red and photographic infrared linear combinations for monitoring vegetation".*J Remote sensing of Environment*: 82(127-150), 0034-4257.

Udelhoven, T., S. van der Linden, et al. (2009). "Hypertemporal classification of large areas using decision fusion." Geoscience and Remote Sensing Letters, IEEE **6**(3): 592-596.

USGS website. http://phenology.cr.usgs.gov/ndvi_foundation.php. Accessed date:

24/01/2012.

Van der Knijff, J., R. Jones, and L. Montanarella. (1999). Soil erosion risk assessment in Italy, European Soil Bureau, European Commission.

Van Leeuwen, W. J. D., A. R. Huete, et al. (1999). "MODIS vegetation index compositing approach: A prototype with AVHRR data." Remote Sensing of Environment **69**(3): 264-280.

Viera, A. J. and J. M. Garrett (2005). "Understanding interobserver agreement: the kappa statistic." Fam Med **37**(5): 360-363.

Viovy, N., Arino O, and Belward A. S. (1992).The Best Index Slope Extraction (BISE): A method for reducing noise in NDVI time-series. Int. J. Remote Sens., 13(8): 1585–1590.

Wang, G., Wente, S., Gertner, G.Z., and Anderson, A. (2002). "Improvement in mapping vegetation cover factor for the universal soil loss equation by geostatistical methods with Landsat Thematic Mapper images." International Journal of Remote Sensing **23**(18): 3649-3667.

Wischmeier, W., and D., Smith. (1978). Predicting rainfall-erosion losses - a guide to conservation planning. AH-537.U.S. Dept. Agr., Washington, D.C.

Yamaguchi, Y., A. B. Kahle, et al. (1998). "Overview of advanced spaceborne thermal emission and reflection radiometer (ASTER)." Geoscience and Remote Sensing, IEEE Transactions on **36**(4): 1062-1071.

Zhang Y, Degroote J, Wolter C, Sugumaran R (2009) Integration of modified universal soil loss equation (MUSLE) into a GIS framework to assess soil erosion risk. Land DegradDev 20:84–91

7.0 APPENDIX

Appendix 1: Field measurement sheet

Data Sheet for Land Cover/Use in Bosumtwi basin							**Sample No:**
GPS	X		**Landuse**		**% vegetation cover**		**Map unit:**
Reading	Y		**Landcover**				

Slope % Class:	**Slope**	**Vegetation type**	**Ground cover**	**Remarks**
Flat 0-2	**Aspect**			
Gently sloping 2-8				
Sloping 8-15	N NE			
Mod. steep 15-25	E SE			
Steep > 25	S SW			
	W NW	**Stage of growth**		

Appendix 2. Dendrograms applied on mean NDVI values (above) and EVI values (below).

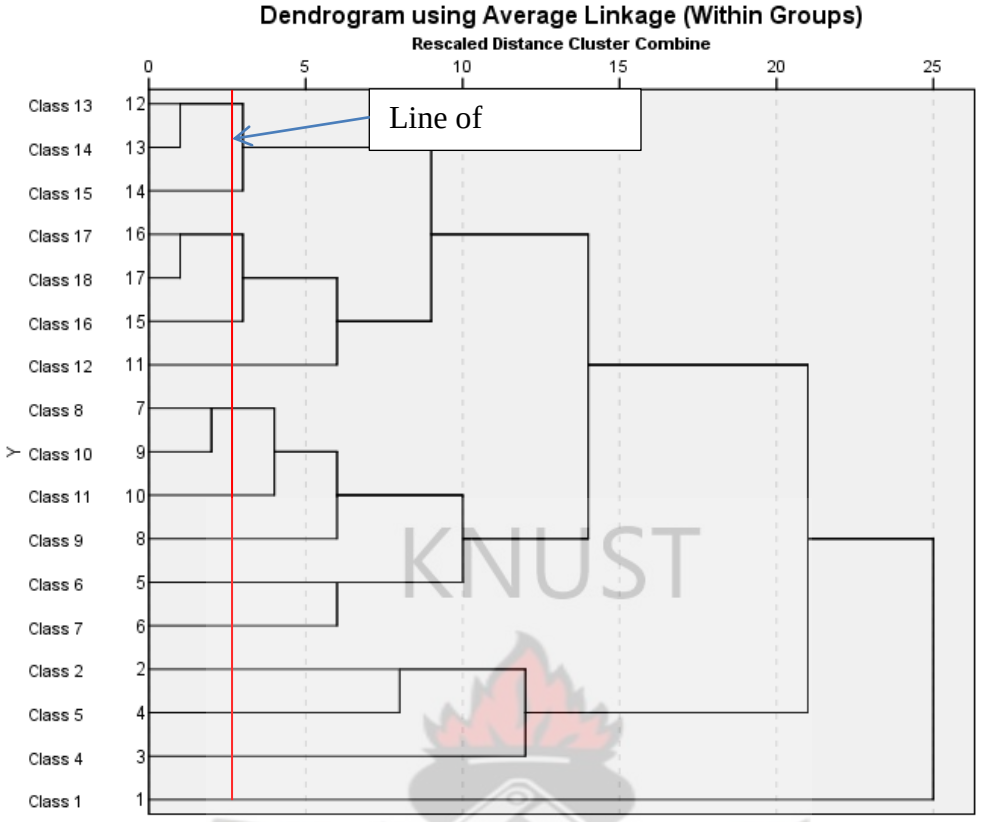

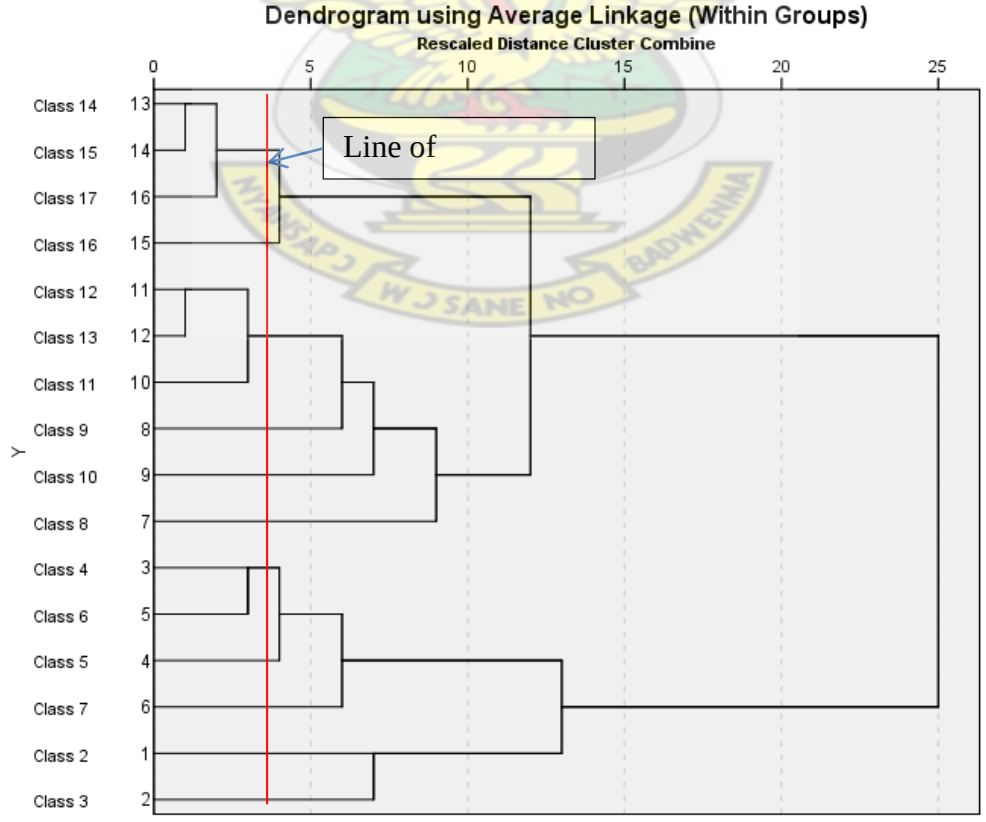

Appendix 3 Profile groups

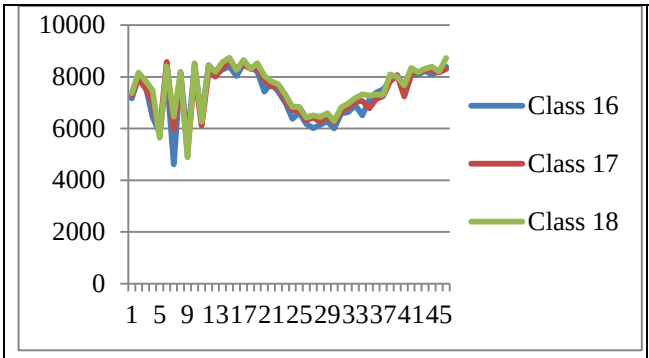

a. NDVI group A {shrub + farmland}

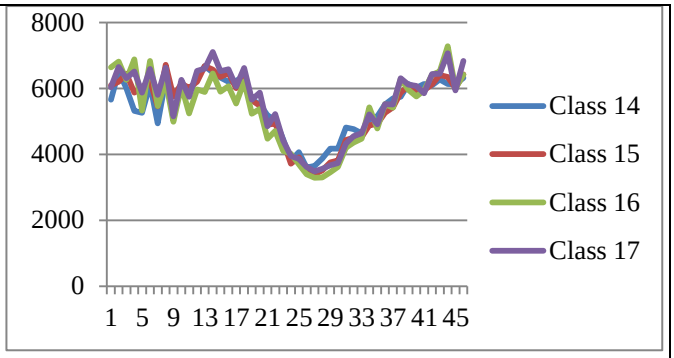

b. EVI Classes group A {shrub + farms}

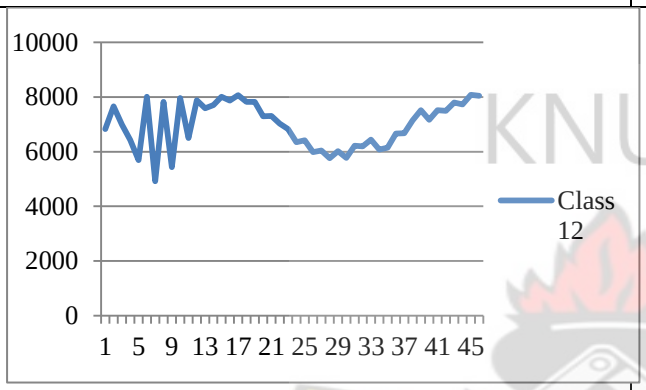

c. NDVI group B {Bare/Grassland}

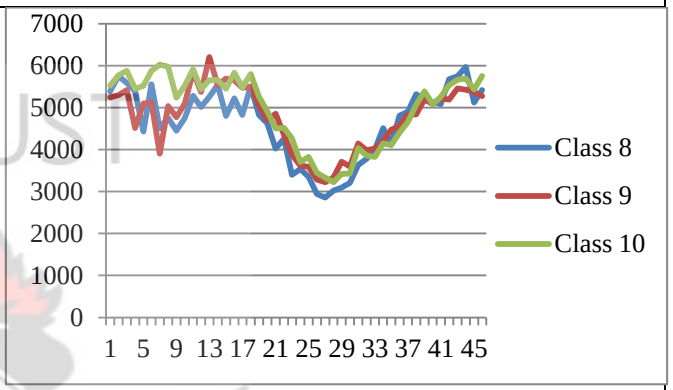

d. EVI Classes group B {Bare/Grassland}

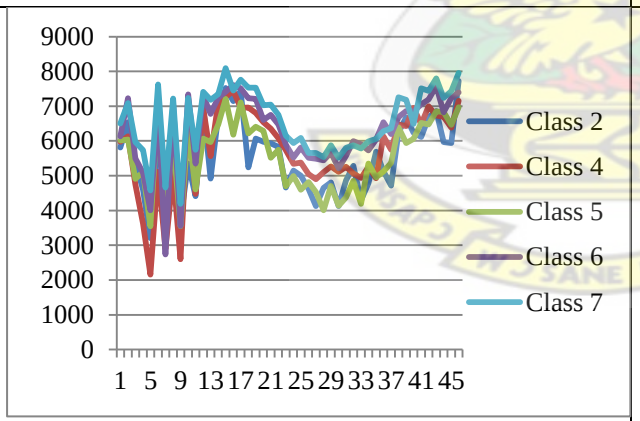

e. NDVI group C {Built up}

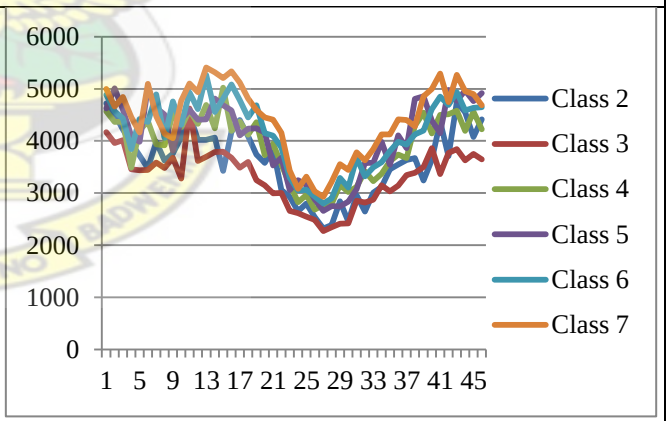

f. EVI Classes group C {Built up}

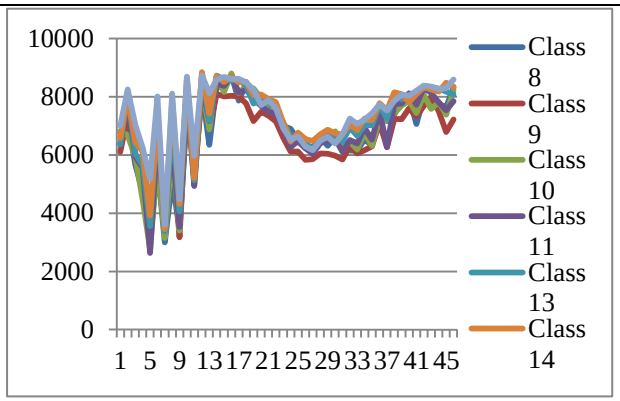

g. NDVI Classes group D {Forests}

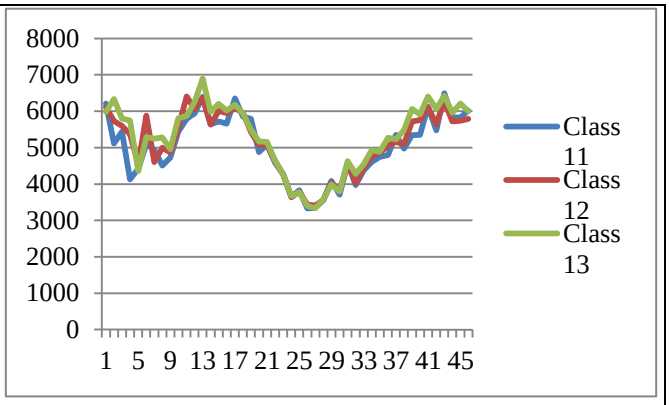

h. EVI Classes group D {Forests}

Appendix 4: MODIS data acquisition dates

No.	Julian days	Calendar days	Calendar days	No.	Julian days	Calendar days	2001
1	177	June 26	26-06	25	001	Jan 01	01-01
2	185	July 04	04-07	26	009	Jan 09	09-01
3	193	July 12	12-07	27	017	Jan 17	17-01
4	201	July 20	20-07	28	025	Jan 25	25-01
5	209	July 28	28-07	29	033	Feb 02	02-02
6	217	Aug 05	05-08	30	041	Feb 10	10-02
7	225	Aug 13	13-08	31	049	Feb 18	18-02
8	233	Aug 21	21-08	32	057	Feb 26	26-02
9	241	Aug 29	29-08	33	065	Mar 06	06-03
10	249	Sep 06	06-09	34	073	Mar 14	14-03
11	257	Sep 14	14-09	35	081	Mar 22	22-03
12	265	Sep 22	22-09	36	089	Mar 30	30-03
13	273	Sep 30	30-09	37	097	Apr 07	07-04

14	281	Oct 08	08-10	38	105	Apr 15	15-04
15	289	Oct 16	16-10	39	113	Apr 23	23-04
16	297	Oct 24	24-10	40	121	May 01	01-05
17	305	Nov 01	01-11	41	129	May 09	09-05
18	313	Nov 09	09-11	42	137	May 17	17-05
19	321	Nov 17	17-11	43	145	May 25	25-05
20	329	Nov 25	25-11	44	153	June 02	02-06
21	337	Dec 03	03-12	45	161	June 10	10-06
22	345	Dec 11	11-12	46	169	June 18	18-06
23	353	Dec 19	19-12				
24	361	Dec 27	27-12				

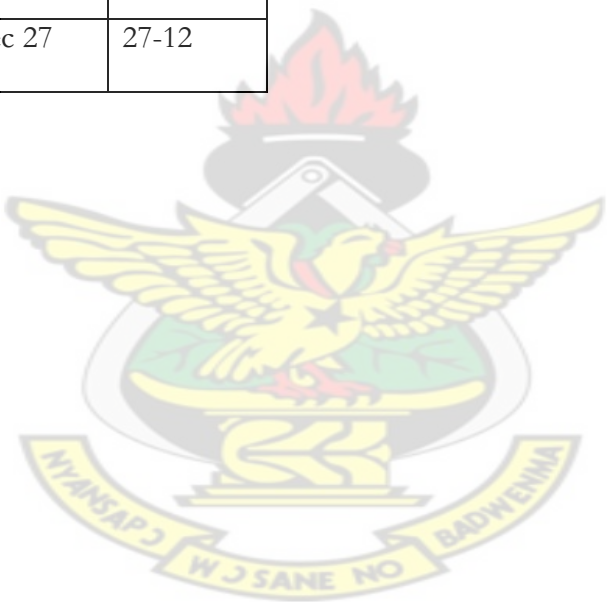

Appendix 5: Distribution of *C* – factors in each cover type

	C factors	*Shrub/Farm*	*Bare/Grassland*	*Built-up*	*Forest*
1	0.0 - 0.1	10.73293	0	0	5.776
2	0.1 - 0.2	481.4018	181.8345	86.26275	875.7942
3	0.2 - 0.3	40.21337	12.71802	70.90318	14.56447
4	0.3 - 0.4	0.015519	3.6	35.06958	0.006215
5	0.4 - 0.5	0.008101	1.6	23.20119	0.000029
6	0.5 - 0.6	0.017165	0	11.68173	0

Appendix 6: First output of NDVI and EVI classification maps (using 21 & 20 maximum number of classes respectively).

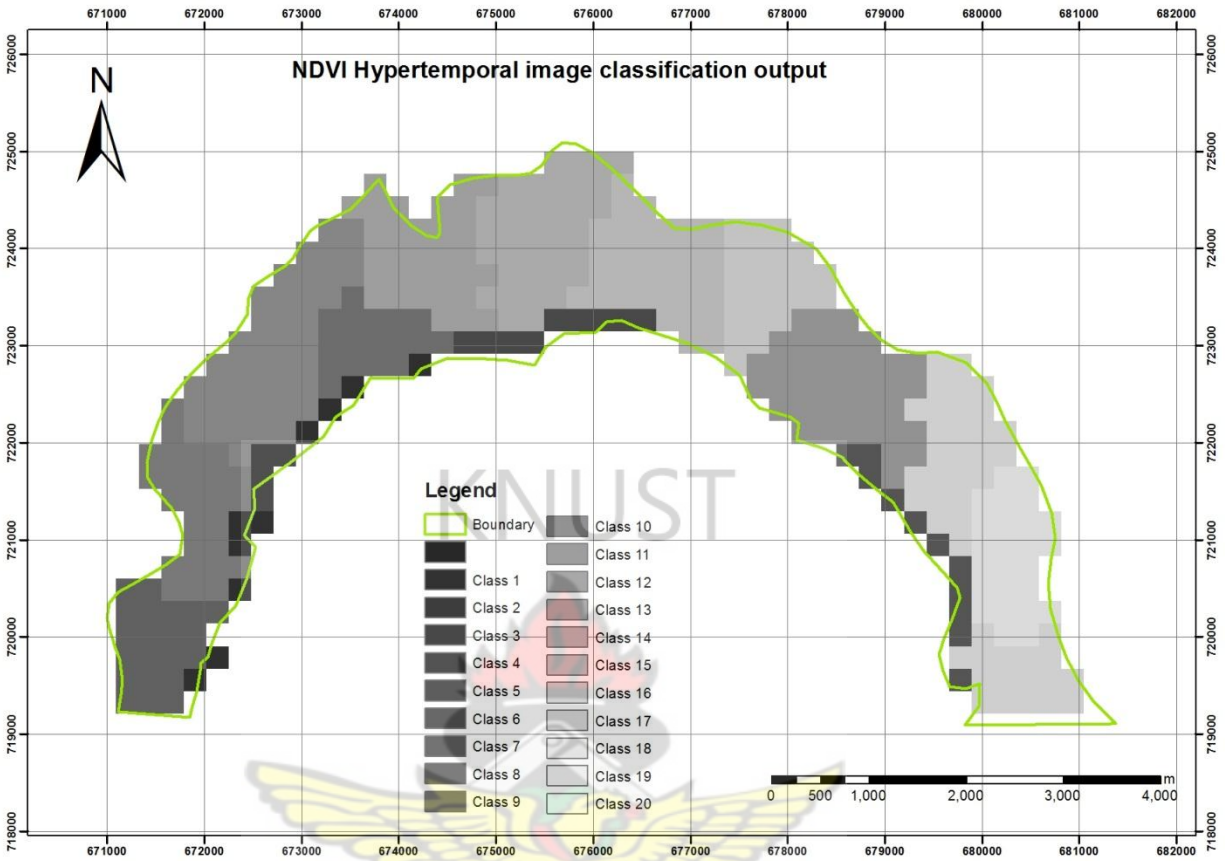

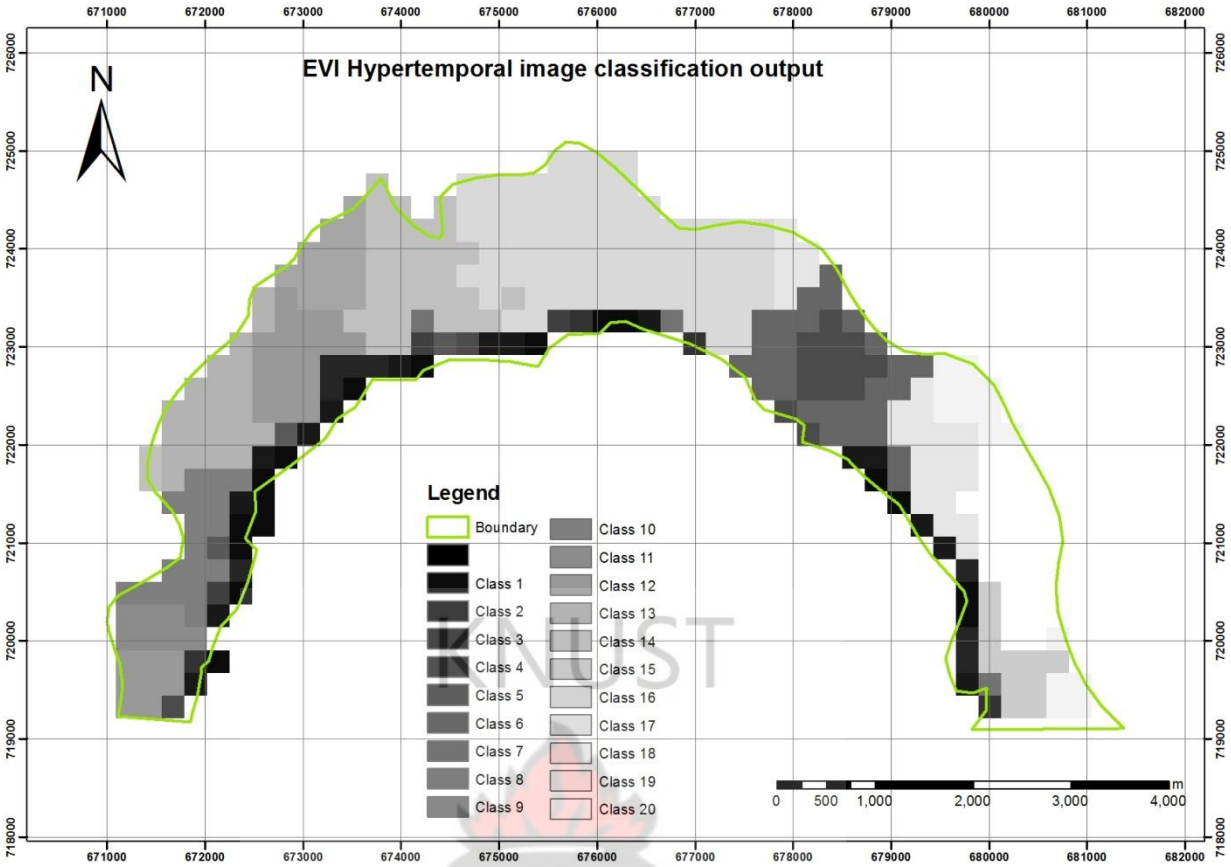
EVI Hypertemporal image classification output
N
Legend
Boundary
Class 1
Class 2
Class 3
Class 4
Class 5
Class 6
Class 7
Class 8
Class 9
Class 10
Class 11
Class 12
Class 13
Class 14
Class 15
Class 16
Class 17
Class 18
Class 19
Class 20
0 500 1,000 2,000 3,000 4,000 m
671000 672000 673000 674000 675000 676000 677000 678000 679000 680000 681000 682000
726000 725000 724000 723000 722000 721000 720000 719000 718000